Lawrence Berkeley Laboratory
UNIVERSITY OF CALIFORNIA

Accelerator & Fusion
Research Division

Presented at the NIRS International Workshop on Heavy Charged Particle Therapy and Related Subjects, Chiba, Japan, July 4–5, 1991, and to be published in the Proceedings

Future Biomedical Research at the Bevalac

J.R. Alonso, W.T. Chu, B. Feinberg, B.A. Ludewigt, T.R. Renner, and J.W. Staples

October 1991

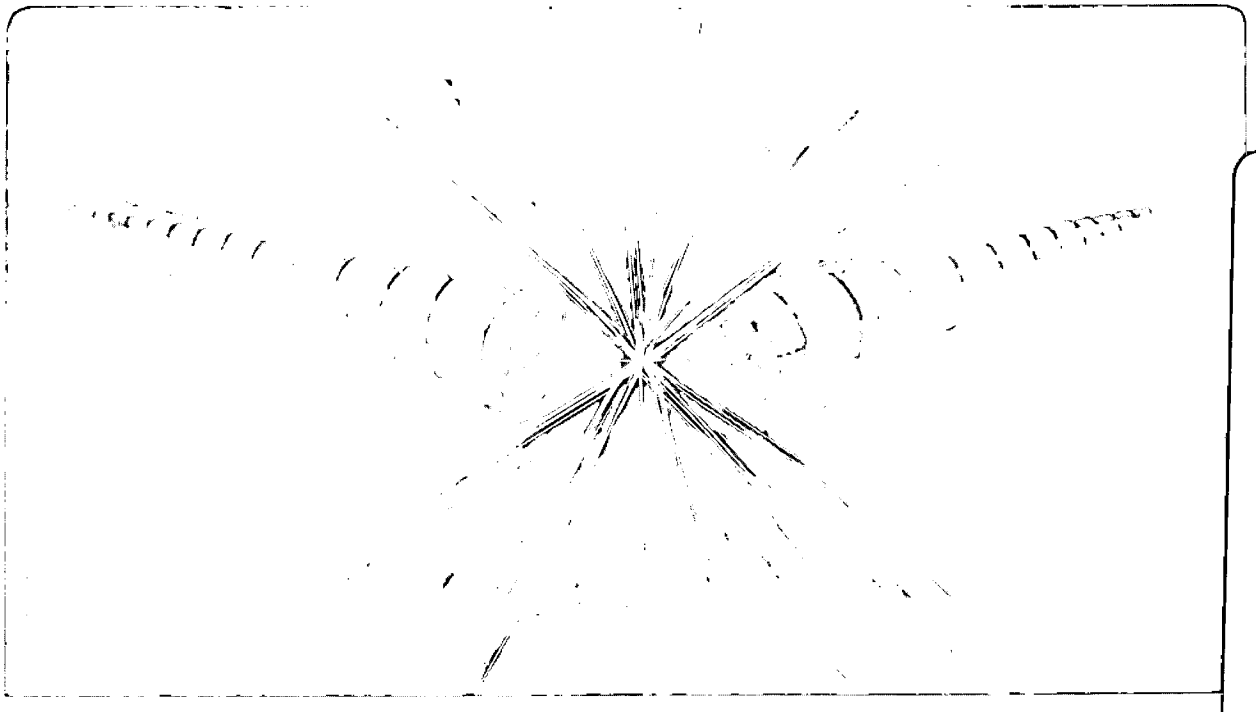

Prepared for the U.S. Department of Energy under Contract Number DE-AC03-76SF00098

DISCLAIMER

LBL-31422

Future Biomedical Research at the Bevalac

J. R. Alonso, W. T. Chu, B. Feinberg, B. A. Ludewigt, T. R. Renner, J. W. Staples

ACCELERATOR FUSION RESEARCH DIVISION
Lawrence Berkeley Laboratory
University of California
Berkeley, California 94720

October, 1991

*This work was supported by the Director, Office of Energy Research, of the U.S. Department of Energy under Contract No. DE-AC03-76SF00098 and in part by the National Institute of Health under Grant CA49562 and CA53835.

FUTURE BIOMEDICAL RESEARCH AT THE BEVALAC*

J. R. Alonso, W. T. Chu, B. Feinberg, B. A. Ludewigt, T. R. Renner, J. W. Staples
Lawrence Berkeley Laboratory
University of California, Berkeley, CA 94720, U. S. A.

In the early 1970s, ions heavier than protons were accelerated[1] in the Bevatron, a weak-focusing synchrotron which was completed in 1954 for acceleration of protons. It enabled the initiation of pioneering studies of biological effects of high-energy light and heavy ions.[2] The construction of the Bevalac accelerator complex,[3] in which the superHILAC injects ion beams into the Bevatron for biomedical as well as nuclear science research, expanded the opportunity for medical studies with heavy charged-particle beams. Clinical trials for treating human cancer using heavier ions have been in progress at the Bevalac since 1975.[4] Ions of clinical interest have ranged from ^{4}He to ^{28}Si; the most commonly used ion has been ^{20}Ne with energies per nucleon of 456 and 585 MeV. Radiation biology and biophysics experimenters use all species of ions ranging from protons to uranium.

At the present time funding for Bevalac operations for all its research programs comes from DOE's Office of Nuclear Physics. Because of changing priorities in nuclear physics, we have been informed that support from this Office for the Bevalac will cease in 1995. Various methods are being investigated for maintaining an accelerated light and heavy ion capability for the biomedical research at LBL. One of these is a proposal to NASA to operate the Bevalac as a cosmic ray factory for space radiation effects research.

The Bevalac presents unique opportunities to NASA because its energetic beams of light and heavy ions can realistically simulate almost all of the cosmic-ray spectrum in a laboratory environment. NASA has taken advantage of this capability for many years by conducting materials studies, calibrating detectors, and performing basic space-science research. In support of planned manned planetary missions beyond the magnetosphere, the program would be expanded greatly into three main areas:

- Radiation biology, studying the effects of HZE (high charge and energy) particle induced mutagenesis and carcinogenesis.
- Materials science, characterizing the effectiveness of shielding materials and the radiation resistance of equipment.

- Space physics, a basic-science corollary of the manned-mission research, seeking to understand the interactions of cosmic rays with, for example, interstellar gas clouds.

This pure and applied research builds not only upon the technical capabilities of the Bevalac, but also upon its existing research program. Present users of the facility, from LBL and elsewhere, would be among the scientists proposing research within the NASA program. Under this proposal, NASA would significantly increase its current low level of Bevalac usage beginning in fiscal year 1992, sponsoring additional operation on nights and weekends during the 22 weeks per year in which the Bevalac is used solely for the therapy program. The total NASA program would ramp up from its current level of about 300 hours of research beam time per year to 1000-plus hours. Meanwhile, the current nuclear-science and biomedical programs would continue. After FY 1994, NASA and NASA-supported research would comprise the entire base program at the Bevalac. Other agencies might purchase additional beam time. Recently NASA has decided to establish a NASA Specialized Center of Research and Training for space radiation health for a Colorado State University/LBL Consortium. The NSCORT will carry out much of its research and training using the light and heavy ion beams at the Bevalac.

With these provisions, the Bevalac could continue in its role as an advanced biomedical research facility well into the next century.

* This work is supported by the Director, Office of Energy Research, of the U.S. Department of Energy under Contract No. DE-AC03-76SF00098 and in part by the National Institute of Health under Grant CA49562 and CA53835.

References

1 H. A. Grunder, W. D. Hartsough, and E. J. Lofgren, "Acceleration of heavy ions at the Bevatron," **Science 174**: 1128-1129 (1971).

2 C. A. Tobias, "Pretherapeutic investigations with accelerated heavy ions," **Radiology 108**: 145-158 (1973).

3 A. Ghiorso,, H. A. Grunder, W. Hartsough, G. Lambertson, E. Lofgren, K. Lou, R. Main, R. Mobley, R. Morgado, W. Salsig, and F. Selph, "The Bevalac: An economical facility for very high energetic heavy particle research," **IEEE Trans. Nucl. Sci. NS-20**: 155 (1973).

4 J. R. Castro, "Treatment of Cancer with Heavy Charged Particles," Lawrence Berkeley Laboratory Report PUB-5301 (February 1991).

LAWRENCE BERKELEY LABORATORY
UNIVERSITY OF CALIFORNIA
INFORMATION RESOURCES DEPARTMENT
BERKELEY, CALIFORNIA 94720

LBL-31426
UC-213
Preprint

Lawrence Berkeley Laboratory
UNIVERSITY OF CALIFORNIA

Materials Sciences Division

Submitted to Journal of Electroanal Chemistry

The Effect of Specific Adsorption of Ions and UPD of Copper on the Electro-Oxidation of Methanol on Pt Single Crystal Surfaces

N. Markovic and P.N. Ross

October 1991

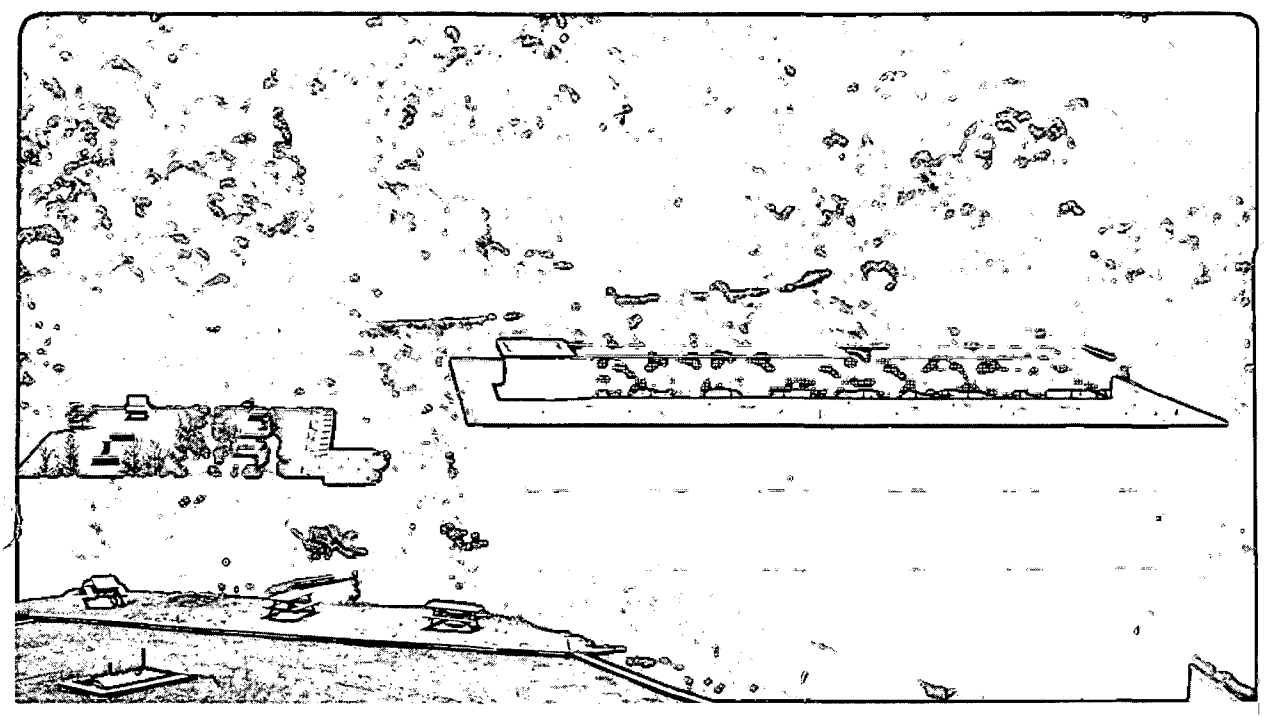

Prepared for the U.S. Department of Energy under Contract Number DE-AC03-76SF00098

DISCLAIMER

LBL-31426

THE EFFECT OF SPECIFIC ADSORPTION OF IONS AND UPD OF COPPER ON THE ELECTRO-OXIDATION OF METHANOL ON Pt SINGLE CRYSTAL SURFACES

Nenad Markovic and Philip N. Ross

Materials Sciences Division
Lawrence Berkeley Laboratory
One Cyclotron Road
Berkeley, California 94720

This work was supported by the Assistant Secretary for Conservation and Renewable Energy, Office of Transportation Technologies, Electric and Hybrid Propulsion Division of the U.S. Department of Energy under Contract No. DE-AC03-76SF00098.

LBL-31426

THE EFFECT OF SPECIFIC ADSORPTION OF IONS AND UPD OF COPPER ON THE ELECTRO-OXIDATION OF METHANOL ON Pt SINGLE CRYSTAL SURFACES

Nenad Markovic* and Philip N. Ross

Materials Sciences Division
Lawrence Berkeley Laboratory
One Cyclotron Road
Berkeley, California 94720

ABSTRACT

The specific adsorption of anions in acid electrolytes containing sulfuric and hydrochloric acids was found to have a strongly inhibiting effect on the rate of methanol electrooxidation on both the (111) and (100) surfaces of Pt. The effect was much stronger in hydrochloric acid, requiring approximately three orders of magnitude higher concentration of sulfuric acid to achieve the same inhibiting effect (and surface coverage by adsorbed anion). Cl^- adsorption isotherms were measured using the emersion technique and ex-situ AES analysis. The mechanism of inhibition appeared to be similar for both anions. On the (111) surface, anion adsorption was found to proceed in two stages, one coupled to hydrogen desorption producing a co-adsorbed state, and a second stage of adsorption at more anodic potentials into the anion adlattice from which hydrogen has been desorbed. The second stage process on Pt(100) is different, occurring at more anodic potentials than on Pt(111) and concurrent with OH formation. Completion of the second stage of adsorption appears to produce the inhibition that causes a current peak to be observed in the voltammetry of methanol in acids containing these anions. Underpotential deposition (UPD) of Cu in acids containing these electrolytes caused strong additional inhibition of methanol oxidation rate. The effect was attributed to induced anion adsorption on Pt atoms near to the UPD Cu atoms due to a lowering of the local pzc by the Cu adatoms.

*Permanent address: Institut of Electrochemistry, ICTM, University of Belgrade, Belgrade, Yugoslavia

1. INTRODUCTION

The oxidation of methanol has been thoroughly studied during the last two decades, mainly in connection with development of fuel cells[1-3]. Most of the earlier studies were carried out on polycrystalline platinum electrode in aqueous solutions[4-6]. In the past few years extensive studies have been undertaken with platinum single crystal surfaces in order to establish the influence of the surface structure on the reaction of the oxidation of methanol. Bagotzky et. al.[7] were the first to report the investigation of methanol oxidation on low-index surfaces of platinum. They found that there was no structural sensitivity for this reaction, however more recently Adzic et. al[8] and Cavilier et. al.[9] found pronounced structural effects in the oxidation of methanol on the low-index and high index planes of platinum[10]. Moreover, recent work with single crystals has clearly shown that the poisoning of the surface that occurs in the course of the oxidation reaction is structure sensitive. There is general agreement that the (111) plane is the least poisoned, with the (100) surface being more susceptible to poisoning probably due to stronger interaction of poisoning intermediates with the (100) surface sites.[11-13] The real nature of the strongly bound intermediates has long been the subject of controversy between different groups. There are two possible candidates as poisoning species: linearly and single bonded CO[14-15] and a formyl species CHO[16-17]. To be completely oxidized to CO_2 those species need to interact with the reactants containing oxygen. Generally it has been accepted that an activated state of water is the source of the oxygen. Based on these concepts an effective catalyst for the oxidation of methanol must adsorb both methanol

and an oxygen-like species at low potentials. Methods used to achieve these properties include the alloying of platinum[18] and the modification of the Pt surface by foreign metal ad-atoms. It has been reported that tin and ruthenium ad-atoms gave an enhancement[2-3] while Pb, Hg, Bi and Cu inhibited the reaction of the methanol oxidation on Pt[19]. It is suggested that if the adsorption of oxygen or hydroxyl radicals occurs on ad-atoms adjacent to the methanolic species, then the catalytic activity for the oxidation of methanol is enhanced. On the other hand, oxidation of methanol is poisoned if the ad-atoms do not adsorb the oxygen-like species. Several studies have attempted to confirm this general model of ad-atom catalysis. Shibata and Motoo[19] reported that Cu inhibited the reaction of methanol on Pt, but could not confirm the absence of water activation. According to Beltowska-Brezinska et. al.[20], Pb ad-atoms were considered to enhance the oxidation of methanol by activating water via a redox process. On the other hand, E. Leiva and M. Giordano[21] reported that ad-atoms having a positive effect on the oxidation of methanol function as "poison blockers". All previous studies, however, have neglected to consider the influence of ad-atoms on the oxidation of methanol by changing the properties of the Pt surface for the adsorption of anions which, as expected, have an inhibitive effect on methanol oxidation. We present here a new mechanism for the effect of Cu ad-atoms on the rate of methanol oxidation related to anion adsorption. Further, we present a new interpretation of the potential dependance of methanol oxidation, that the anion adsorption and not "oxide" formation[4,6] controls the shape of the voltammetry curves for the oxidation of methanol on low-index single crystal surfaces of platinum.

2. EXPERIMENTAL

The platinum single crystals used in these studies have been prepared by two different methods. The first of these methods involves ultrahigh vacuum (UHV) preparation and characterization and the other involves preparation ex-vacuo in an open hydrogen flame. The UHV-electrochemistry system has been described in detail elsewhere[22]. Surface cleanliness was monitored by Auger Electron Spectroscopy (AES) and the surface structure determined using LEED. Within the sensitivity limits of AES there were no detectable surface impurities before transfer to the electrochemical chamber. LEED patterns on the clean, annealed surface were characteristic of a well ordered surface. After UHV preparation and characterization, the single crystal was transferred into an electrochemical environment using technique designed to minimize the possibility of contamination[22]. Following electrochemical characterization, the single crystal was emersed from the electrolyte and returned to the ultrahigh vacuum environment for post-electrochemical analysis.

For analysis of emersed electrodes by AES, special precautions were taken to avoid electron beam stimulated desorption of Cl species. These involved defocussing and rastering the electron beam over an approximately 0.3 × 0.3 cm area while using the minimum beam current (e.g. 1 μA) that produces a useable signal, and recording only the energy region from 150-250 eV for the Cl isotherms. Calibration of the absolute Cl coverage from the Cl (181)/Pt(237) AES peak ratios was accomplished using UHV dosing of the Pt(100) surface with HCl to produce the c(2 × 2) LEED

pattern[35]. The coverage for this pattern was assumed to be the ideal 1/2 monolayer value, 5×10^{14} atoms/cm^2. Calibration of the Cu coverage was from the Cu (920)/Pt (237) peak ratio for a monolayer of Cu evaporated onto Pt(111) in UHV[34].

The flame technique for the preparation of large single crystals has also been discussed in detail previously[23]. This procedure involves heating single crystals in hydrogen-air flame. The crystals are then cooled in closed pyrex tube purged with flowing hydrogen. After cooling a drop of ultra-pure water is placed onto the crystal surface. The thin film of water protects the surface from contamination during the through-air transfer into the electrochemical cell.

In the present study the electrochemical cell also serve as an external electrolyte reservoir from which the electrolyte is delivered into the UHV-electrochemical chamber. This allowed us to perform the experiment with the same electrolyte using the same crystal orientation but using crystals prepared by the two different methods. A comparison of the results of flame annealed and UHV-prepared Pt(111) single crystals obtained in 0.1 M$HClO_4$ with and without methanol is shown in Fig. 1. The results of flame annealed and UHV prepared single crystals are essentially identical, confirming that relatively simple and fast flame technique provide a high-quality surface. Most of the results reported here were obtained with the flame annealed crystals. Results with UHV prepared surfaces are noted specifically.

Electrolyte solutions were prepared using concentrated $HClO_4$, H_2SO_4 and HCl (all ultra-grade, J.T. Baker). The water used was pyrolitically, triply distilled water. The copper solution was prepared by dissolving CuO in 0.1 M$HClO_4$.

The reference electrode used was a Pd-H wire. All potentials in this study, however, will be quoted according to the reversible hydrogen electrode in the same electrolyte (RHE). The physical surface areas for the flame-annealed Pt(111) and Pt(100) crystals were 0.568 cm^2 and 0.572 cm^2, respectively. The contact area of the electrolyte drop on the crystal surface in the thin layer cell was approximately 0.35 - 0.45 cm^2.

The voltammograms were recorded with a sweep rate of 50 mV cm^{-1} except where noted.

3. RESULTS

3.1 Cyclic Voltammetry in $HClO_4$ and H_2SO_4

The effect of the acid anion on the rate of methanol oxidation on both Pt(111) and (100) surfaces is easily seen in the voltammetry curves of Figure 2. There are two characteristics of the anodic waves for methanol oxidation that represent the anion effect. The first is that the current densities at the same potentials are much higher in $HClO_4$ than in H_2SO_4 of the same pH on both (111) and (100), presumably due to a greater extent of anion adsorption in the latter electrolyte. The inhibition appears to be somewhat greater on (111) than on (100). This observation is not new, and has been reported by Clavilier and co-workers[9]. The second characteristic, which has not been noted specifically before, is that the peak maximum for methanol oxidation on (111) in H_2SO_4 occurs at a potential which is at least 0.4 V cathodic of the potential for "oxide" formation! Clearly, the decrease in the methanol oxidation current above 0.6 V cannot be due to the formation of inhibiting "oxide" species, at

least in the case of the (111) surface. The methanol oxidation peak is located at a potential which in methanol free solution corresponds to a small pseudo-capacitive feature which one sees in even the earliest curves by Clavilier for Pt(111)[29] but is rarely discussed. We shall discuss our interpretation of this feature in a later section. In $HClO_4$, the methanol oxidation peak on (111) is located at a potential which in methanol-free electrolyte corresponds to the center of the "anomalous" feature, anomalous in the sense that the processes associated with this feature are not understood or about which there is controversy (see the discussion in Wagner and Ross[38]). The interpretation of the process which causes the shape of the methanol oxidation current wave is coupled to the interpretation of the anomalous feature in methanol-free voltammetry as will be discussed in the next section.

The methanol oxidation current peak on Pt(100) occurs at a potential which in methanol free-electrolyte is at a minimum in the double layer capacity, but is just cathodic to the onset of "oxide" formation in both $HClO_4$ and H_2SO_4. However, in both electrolytes, the amount of "oxide" seems incredibly small to be related to such large inhibiting effect, e.g. the current drops by one order of magnitude over a potential range where the integral charge is less than 10 $\mu C/cm^2$, approximately 5% on an OH monolayer. Therefore, we present an hypothesis that the shape of methanol oxidation wave on Pt(100) in both $HClO_4$ and H_2SO_4 is mainly determined by the processes and chemistry of anion adsorption.

3.2 The effect of $(OH)_{ads}$ species

One of the approaches we employed in the present work to elucidate which species might be causing the inhibition of methanol on Pt(111) was to add intentionally selected candidate ions/molecules and observe their effect. An obvious candidate ion is OH^-, since OH has been suggested by several groups as a species involved in the anomalous feature[36,42]. The role of adsorbed OH in methanol oxidation is easily observed simply by comparing the voltammetry in KOH with and without methanol, as done in Figure 3. As was the case in the acid electrolyte, the inhibition of methanol oxidation takes place at the potential corresponding to completion of the process (es) involved in the anomalous feature. Since there is general agreement that the anomalous feature on Pt(111) in KOH is caused by specific adsorption of OH^-[36,42], one can reasonably conclude that on Pt(111) adsorbed OH produced by specific adsorption of OH^- is actually an inhibiting rather than a catalyzing species, a surprising result.

The results on Pt(100) with respect to the role of OH^- on the shape of methanol oxidation wave are less clear than on Pt(111). As was the case for Pt(111) in KOH, the peak maximum for methanol oxidation on Pt(100) occurs where in methanol free-electrolyte appears a small pseudo-capacitive feature which according to recent results[42] are attributed to specific adsorption of OH^- species. It therefore appears that OH^- adsorption in the "double layer" potential region of Pt(100) also has an inhibiting effect on the methanol oxidation, as will be discussed in detail elsewhere[41].

3.3 The Effect of Chloride

3.3.1 Influence of Traces of Chloride Impurities on the Anomalous Feature on Pt(111)

There was a clear indication in unpublished work by Markovic and Yeager[31], reproduced in Figure 4, that at least part of the anomalous feature is associated with Cl^- adsorption, the latter being present as an impurity in $HClO_4$ at a concentration of at least 10^{-7} M in even the most meticulously prepared electrolyte[37]. As seen in Figure 4, the addition of HCl to $HClO_4$ in trace amounts produced a sharpening of one of the features in the anomalous region, implying that Cl^- adsorption may be one of the process producing the anomalous capacitance in $HClO_4$. Thus, the shape of methanol oxidation wave on Pt(111) in $HClO_4$ seems to be determined by the blocking effect of both specifically adsorbing Cl^- and OH^- species.

3.3.2 Chloride AES Isotherm for Pt(111)

We sought to confirm the possible role of a Cl^- impurity by means of ex-situ analysis of the emersed Pt(111) surface with Auger electron spectroscopy (AES), thermal desorption spectroscopy (TDS), and low energy electron diffraction (LEED)[22]. Unfortunately, these emersion experiments are not meaningful when $HClO_4$ is used as the electrolyte. The emersed surfaces of Pt retain not only the double-layer, but also a viscous boundary layer of bulk electrolyte which crystallizes on the electrode surface when exposed to vacuum if the solute molecule is not volatile[22], which is the case for $HClO_4$. The emersion experiments were therefore done with 0.3 M HF as the electrolyte, since HF and HCl is a volatile solute and the

voltammetry of Pt(111) in dilute HF and $HClO_4$ are essentially identical. Cl was clearly seen in the AES spectra of Pt(111) emersed from 0.3 M HF (no HCl added intentionally) at all potentials, with a potential dependance (Figure 5) that shows two states. The states became more easily distinguished when HCl was added to the HF. When HCl was added to 10^{-5} M, the voltammetry curve changed as noted and the Cl AES isotherm clearly showed two states, one adsorbing at ca. 0.3 V and another at ca. 0.7 V, and both states produce distinct capacitive features in the voltammetry curve at these potentials. Since additions of HCl to the level of 10^{-6} M produced no observable changes in either the Cl AES isotherm or the voltammetry curve, we concluded that the level of Cl in our HF electrolyte was ca. 10^{-6} M, consistent with the level of Cl impurity reported by the supplier of the concentrated HF (Baker, Ultrex Grade). The absolute coverages of Cl were calculated from the AES peak ratios and they appear to be quite low for emersion from 10^{-5} M Cl electrolyte. However, both the shape of the AES isotherm and the absolute coverages are in reasonable agreement with the radiotracer results of Horanyi et. al. for polycrystalline Pt in 0.1 M $HClO_4$ + 10^{-5} M HCl.

The potential dependence of the AES isotherm suggests a two-stage process for chloride adsorption, the first chloride adsorption coupled with hydrogen desorption, the second adsorption onto a H-Cl adlattice from which H has been removed anodically creating additional sites for chloride adsorption. The concentration dependance of the AES isotherm is also consistent with this two-stage picture, since the stage coupled with hydrogen is a competitive process between chloride ions and

protons, the latter being in a huge excess in 0 .1 N $HClO_4$ + 10^{-5} HCl. From such a dilute solution, chloride cannot compete with protons for the surface, and the majority of chloride is adsorbed at more anodic potentials where adsorption of hydrogen is thermodynamically unfavorable. It should also be noted that the potential of zero charge (pzc) for Pt(111) in 0. 1 N $HClO_4$ is estimated to be at 0.6 - 0.7 V[28]. This is consistent with the major state of chloride adsorption from very dilute solution (10^{-6} - 10^{-5} M Cl^-) being near the pzc.

3.3.3 Chloride AES Isotherm for Pt(100)

The AES isotherm for Pt(100) emersed from 0.3 M HF is shown in Figure 6, along with the corresponding voltammetry. The potential dependance is simpler on (100) than on (111), there is only one stage of adsorption apparent in the potential region below 0.8 V, that being a process coupled to hydrogen desorption. This isotherm is consistent with the pzc for the (100) surface being ca. 0.4 V cathodic of that for the (111) surface[28]. The coupling of chloride adsorption with hydrogen desorption produced a significant change in the pseudo-capacity in the potential region between 0 - 0.4 V, even at the very low concentration of 10^{-5} M. There was a second stage of adsorbed chloride, but this was not the same as the second stage of adsorption on the (111) surface. On (100), there was a state of Cl co-adsorbed with oxygen species that started to form at potentials above 0.8 V. This was actually opposite the behavior of the (111) surface, i.e. on (111) the onset of formation of oxygen species above 1.0 V

caused the surface coverage of Cl to decrease. This second state of chloride adsorption was also evident in the voltammetry curve, by the enhanced pseudocapacity at ca. 1.0 V.

3.3.4 Influence of the Concentration of Chloride on Methanol Oxidation

The emersion experiment confirmed that HF contains Cl^- as an impurity, possibly at a level high enough to affect the electrochemistry as suggested in earlier work by Markovic et. al.[23]. There are claims in the literature[31,37] that even the purest commercially available $HClO_4$ contains sufficient Cl^- impurity to affect the electrochemistry of Pt and Au. To examine the possible effect of Cl^- impurities on the rate of methanol oxidation in our $HClO_4$, we compared the kinetics for both Pt(111) and (100) in $HClO_4$ versus HF at the same pH. The results for HF are shown in Figure 7, and should be compared to the results in Figure 2 for $HClO_4$. The shapes of the curves in HF are very different from those in $HClO_4$, particularly for Pt(100), a difference we attribute to the higher level of Cl^- in HF versus $HClO_4$. HCl was added to the $HClO_4$ until the methanol oxidation waves coincided with those in HF, which occurred for a level of about 2×10^{-5} M HCl, as shown in Figure 8 for continuous cycling. This was a surprisingly high level, several times higher than in other results with HF, e.g. Figures 5 & 6, and more than an order of magnitude higher than expected from the manufacturer's claimed level. We attributed this variation in apparent magnitudes of Cl^- impurities in HF to lot-to-lot variations in the commercial HF.

The effect of Cl^- on the rate of methanol oxidation could be seen by examining the results for additions of Cl^- near the threshold level, as shown in Figure 9. The curves shown are for the first anodic sweep after immersion at 0.2 V. There was a threshold amount of ca. 5×10^{-6} M before an effect was seen, then increasing the Cl-concentration to 5×10^{-5} M shifted the onset potential for methanol oxidation and the potential of the current maximum also shifted anodically with respect to the wave without Cl-added. Comparison of the methanol oxidation current wave for Pt(111) with the Cl adsorption isotherm in Figure 5 indicates that the potential of the current maximum corresponds to the onset of the Cl adsorption in the 0.8 V state described above. The shift in the onset potential appears to be associated with the Cl adsorption (as seen in the AES isotherm of Figure 5) which is predominent over the adsorption of methanol molecules. Fig. 9 shows that adsorbed Cl^- also has effect on the adsorption pseudocapacity corresponding to the hydrogen adsorption/desorption processes (insert of Fig. 9). However, the effect of adsorbed Cl on the adsorption pseudocapacity in this region is indirect. Trace levels of Cl^- have no observable effect on this pseudocapacity in the absence of methanol, as shown by Figure 4. The indirect effect of trace levels of Cl^- is thus a blocking of methanol adsorption in this potential region, which produces a slight increase in hydrogen adsorption pseudocapacitance. This effect was even more pronounced on the (100) surface where in the hydrogen region Cl adsorption/desorption is coupled to hydrogen desorption/adsorption (isotherm in Figure 6) causing the asymmetry between the anodic and cathodic sweeps (insert of Figure 9 right). On (100), the effect of Cl was generally more complicated than on

(111), showing a strong dependance on the number of sweeps through the potential region shown, with the inhibition becoming stronger with each successive sweep. This "aging" effect appeared to be related to both the stronger adsorption of Cl on Pt (100) than on Pt(111) and to the lower work function of (100) than (111) surface, requiring a lower potential to desorb the Cl^- ion from (100) vs (111) surfaces. The strong adsorption of Cl^- on (100) has a profound effect on the methanol oxidation current, as shown in Figure 8. On the cathodic sweep from 0.9 V, the (100) surface was essentially completely inhibited by the adsorbed Cl, which starts to be desorbed below 0.4 V. However, due to relatively slow diffusion of Cl^- away from the surface to reproduce the same methanol oxidation current wave on the next anodic sweep, the potential must be held at 0 V for ca. 30 sec. On (111) in the presence of Cl, the methanol oxidation currents show more hysteresis than in Cl^- free electrolyte, but the anodic waves can be reproduced without a potential hold to desorb Cl because Cl^- desorption from the (111) surface occurs at a more positive potential.

3.4 The Effect of Sulphric Acid Anions

The effect of sulfate on methanol oxidation currents is shown in Figure 10. The effects were qualitatively similar to the effect of Cl, but a concentration approximately three orders of magnitude higher was needed to produce the same magnitude of effect (Figure 11). Presumably this was due to a lower heat of adsorption for (bi)sulfate versus chloride anion. An interesting feature of the inhibition by (bi)sulfate is that the effect is actually much larger on (111) than (100), which is the opposite of the effect of Cl^- and also is counterintuitive. As with Cl^-, the shape of the methanol

oxidation wave in sulfuric acid can understood in terms of the (bi)sulfate anion adsorption isotherm. In this case, we refer to the in-situ isotherm reported by Faguy et. al.[27] for Pt(111) obtained with IR spectroscopy. A qualitatively similar isotherm was reported by Wieckowski et. al[39] using the radiotracer technique. The shape of the (bi)sulfate isotherm is similar to the AES chloride isotherm at 10^{-5} M Cl^- reported here (Fig. 5), including two states, one coupled to hydrogen desorption and one adsorbing at the pzc and above. The adsorption of (bi)sulfate anion at 0.2 - 0.4 V appears to correlate with the anodic shift in the onset potential for methanol oxidation, and the continued adsorption at and above the pzc to saturation of the surface appears to correlate with the inhibition at 0.7 - 0.9 V. An adsorption isotherm has not yet been reported for Pt(100) in sulfuric acid, so it is not possible to correlate the effects to known adsorption behavior for this surface. The strongly inhibiting effect of (bi) sulfate anion on the (111) surface versus the (100) surface appears to be due to the tetrahedral geometry of the anion adsorbed on the (111) surface indicated by the IR spectra[27].

3.5 The Effect of UPD of Cu^{2+}

The effect of additions of a metal cation, Cu^{2+}, to the different acid electrolytes is shown in Figs. 12 & 13 for a concentration of 10^{-6} M. A complete discussion of Cu underpotential deposition (UPD) on Pt single crystal surfaces will be presented elsewhere. For our purposes here, where we are focussing on the effects of anion adsorption, we present results that relate specifically to such effects. At a concentration of 10^{-6} M, the amount of Cu electrodeposited in the potential region

shown was quite small (ca. 30 $\mu C/cm^2$ or roughly 5% of a fully discharged Cu monlayer), as measured either by the charge under the anodic stripping peak or (less accurately) by the change in pseudo-capacity in the hydrogen adsorption potential region. The effect of Cu deposition on the rate of methanol oxidation depended on the electrolyte, a nearly insignificant effect in H_2SO_4, but a significant inhibition in $HClO_4$ acid, especially for the (111) surface where the rate at 0.7 V decreased by a factor of 3-4. Such a large kinetic effect cannot be explained by simple site blocking by Cu adatoms.

A possible explanation for the unusually large inhibiting effect of UPD Cu at low coverage lay in a coupling of anion adsorption and Cu deposition. To examine this phenomenon directly, we again used HF as the supporting electrolyte (containing Cl^- as an impurity), with UHV analysis of emersed electrodes. Table 1 summarizes the AES data for the analysis of a (111) electrode emersed from 0.3 M HF + 10^{-6} M Cu^{2+} at 0.3 V, an experiment comparable to that in $HClO_4$ in Figure 8, where coulometry indicates a coverage by UPD Cu on the order of 5% of a metallic Cu monolayer is expected (ca. 20-30 $\mu C/cm^2$). The AES analysis for Cu was in reasonable agreement with that expected from coulometry. The corresponding value of the Cl coverage in the absence of Cu^{2+} in the electrolyte is given in Figure 3, ca. 2×10^{13} atoms/cm^2 at 0.2 - 0.6 V. Comparison of this Cl/Pt ratio (about 0.01) in the absence of Cu^{2+} with that in Table 1 in the presence of Cu^{2+} shows an approximately ten-fold increase in the Cl/Pt ratio due to the presence of the UPD Cu. The Cl/Cu atomic ratio in Table 1 far exceeds that expected for any known Cu-Cl compound, so one can

reasonably conclude that the presence of the UPD induces Cl adsorption onto nearby Pt surface atoms, accounting for the large increase in Cl/Pt ratio in the presence of UPD Cu.

4. DISCUSSION

4.1 The Role of Anions

Methanol oxidation on Pt single crystal surfaces clearly shows that new insight into electrode processes is gained due to the elimination of surface heterogenity and the enhancement of the resolution in voltammetry that results. This is especially true of the (111) surface, where the surface homogeneity results in collective interactions in anion adsorption which are not evident on an atomically rough surface, even with the same orientation[36]. In our study here, the voltammetry of the Pt(111) surface in sulfuric acid solutions containing methanol make it clear that the shape of the methanol wave, with the formation of a current maximum that is kinetically controlled, is not caused by inhibition due to "oxide" formation on the Pt[4-6]. Rather, the inhibition above a certain potential appears to be related to the potential dependence of the adsorption of anions in the electrolyte which interact strongly with the Pt surface, such as Cl^- and HSO_4^- (SO_4^-). In the case of sulfuric acid electrolyte, this relation is evident by reference to the adsorption isotherm for (bi) sulfate on Pt(111) obtained by IR spectroscopy (also by radiotracer), and by the manifestation of (bi) sulfate anion adsorption as pseudo-capacitance in the voltammetry curves themselves. The latter was shown in Figure 14, where it is clear that adsorption occurs in two stages, the first being specific adsorption ca. 0.2 - 0.3 V negative of the pzc, and a second stage at and

positive to the pzc. This second stage, at ca. 0.6 V in 0.05 M H_2SO_4, produces a small but observable pseudo-capacitance, approximately 20 $\mu C/cm^2$ of charge (see Fig. 7), which has the same concentration dependence of peak potential as the first stage feature[30]. The second appears to correspond to a filling in of the anion superlattice formed by specific adsorption, which must have empty Pt sites or else methanol oxidation could not take place at all. Methanol does not appear to compete effectively with (bi) sulfate anions for the Pt(111) surface (at these relative concentrations), because even in the presence of methanol the pseudo-capacitance for specific adsorption is still seen in the voltammetry. The oxidation of methanol proceeds, in the potential region 0.5 - 0.7 V, on the Pt sites not blocked or inhibited by the specifically adsorbed anions, but at higher potentials, positive to the pzc, the driving force for anion adsorption increases, further inhibiting methanol adsorption. Because anion adsorption is kinetically a fairly reversible process, there is little or no hysteresis on the reverse sweep, and the stages of anion adsorption and competition with methanol are reversed in sequence.

4.2 The Analysis of AES Isotherms for Cl^- on Pt(111) and Pt(100)

The availability of true adsorption isotherms for (bi) sulfate on Pt(111) made it possible to establish a direct correlation between voltammetry features and anion adsorption processes and effects, but such isotherms are not available for the (100) surface, nor for Cl^- on either surface. For the (100) surface, we can extrapolate the behavior described above for the (111) surface to the (100) using the electrostatic model for anion adsorption put forth in a previous paper[28], based on the difference

in work function between the (111) and (100) surface. In the case of Cl^- adsorption, we will suggest a very similar role for Cl^- emerges if one assumes that the AES isotherms from emersion experiments are in fact ion adsorption isotherms. For (bi) sulfate on Pt(100), one might postulate a rigid shift of the isotherm to lower potential, by an amount equal to the difference in vacuum work function between (111) and (100), which is about 0.2 eV[28]. Referring to Figures 2, 5 and 10, the extra capacitance near 0.4 V seen in H_2SO_4 versus $HClO_4$ is due to specific adsorption of (bi) surface anion shifted down ca. 0.2 V from the (111) surface, which would be the expected pzc for (100) based on the work function. As with the (111) surface, the maximum in the methanol oxidation current corresponds to the potential where the second stage of anion adsorption is complete, indicated by the pseudo-capacitive feature at ca. 0.6 V. The second stage of anion adsorption causes a strong inhibition of the reaction at potentials above 0.6 V.

The determination of states and coverages of ions and molecules on electrode surfaces by ex-situ analysis of emersed electrodes is still a controversial subject, and we do not claim that the AES isotherms reported here for Cl^- on Pt(111) and (100) are definitively Cl^- adsorption isotherms. We are aware, in fact, of a significant problem with this technique, the chemisorption of HCl after emersion and during evacuation/ transfer to UHV for surface analysis. The source of HCl was from the bulk electrolyte remaining on the surface after emersion. One can only observe electrosorbed Cl if it is at a higher coverage than from the chemisorption of HCl, which will depend on a variety of factors, both thermodynamic and kinetic. The

chemisorption of HCl is evidenced by a potential independent Cl coverage, and is a non-electrochemical state that can be produced just by dosing the surface in UHV with HCl. At HCl concentrations of 10^{-2} M and higher, we observed on the emersed electrode in vacuum Cl which appeared to be due entirely to HCl chemisorption. The coverages and LEED patterns on both (111) and (100) electrodes emersed at these relatively high concentrations of HCl were essentially identical to those reported by Garwood and Hubbard[35] for dosing clean surfaces in UHV with HCl to saturation. From dilute solutions, such as the HF containing less than 10^{-4} M HCl, we did observe potential dependent Cl coverages by AES, indicative of electrosorbed Cl. The shape of this potential dependance for the (111) surface was very similar to that reported by Horanyi and co-workers[38] for polycrystalline Pt in 0.1 M $HClO_4$ + 10^{-5} M HCl using the in-situ radiotracer method. The shape of an isotherm formed by addition of our (111) and (100) AES isotherms would also have the same shape as the radiotracer isotherm. The absolute values of the coverages are also in reasonable agreement with the radiotracer values. We feel it is reasonable to conclude that the AES Cl isotherms reported here may be representative of the true Cl adsorption isotherms for (111) and (100) Pt in solutions containing less than 10^{-4} M Cl^-.

4.3 The Role of UPD of Copper

The inhibiting effect of Cu UPD on the rate of methanol oxidation should be discussed in the light of enhancement of anion adsorption by Cu deposition. An enhancement in Cl adsorption on Pt in the presence of Cu^{2+} in solution was also observed previously in the radiotracer work by Horanyi and co-workers[40]. They also

observed an enhancement in (bi)sulfate adsorption due to Cu^{2+}, a phenomenon we only inferred here from the effects of Cu UPD on the rate of methanol oxidation. They did not discuss this observation in terms of a UPD state of Cu on the Pt surface, but rather simply referred to it as "simultaneous adsorption". One of the difficulties those workers had in explaining this simultaneous adsorption phenomenon was the anion/Cu ratio, which was as high as 4-5. Clearly, ratios this high imply that the electrodeposited Cu not only has at least one anion associated with it, but additional anion adsorption is "induced" onto the Pt surface. We suggest a mechanism for this induced anion adsorption in terms of the local work function concept, and the local pzc, introduced in a previous paper[28]. The deposition of Cu onto Pt lowers the work function of Pt atoms within a Fermi-Thomas screening length of the Cu atom, or essentially every nearest Pt atom to the Cu site. The magnitude of the work function lowering will depend on the state of charge of the Cu, and other details of the adatom-metal surface interaction, i.e. the local dipole moment. From the direct relation of the local work function and the local pzc established previously[28], the local pzc of Pt atoms near the Cu adatom is negative with respect to Pt atoms far away, i.e. the atoms near the Cu are charged positive with respect with atoms far away, resulting in more anion adsorption at these sites at a given electrode potential than on other sites far away from the Cu atom. This mechanism explains the high anion/Cu ratios observed both in our work and in that of Horanyi and co-workers, and also the anomalously large inhibition by very small amounts, e.g. 5% of a monolayer, of UPD Cu on methanol oxidation in electrolytes with specifically adsorbing anions.

5. CONCLUSIONS

In the present study it has been shown that the shape of the methanol oxidation wave on both Pt(111) and Pt(100) appears to be related predominately to the potential dependence of the adsorption of anions such as Cl^- and HSO_4 ($SO_4^=$), which interact strongly with the platinum single crystal surfaces.

In $HClO_4$, the methanol oxidation peak on Pt(111) is located at a potential which in methanol free electrolyte corresponds to the center of the "anomalous" feature. Within the "anomalous" potential region the main reaction appears to be OH_{ads} formation coupled to the adsorption of Cl^- producing a sharp peak at 0.7 V. Both specifically adsorbed Cl^- and OH_{ads} species have an inhibiting effect on methanol oxidation. The methanol oxidation current peak on Pt(100) occurs at a potential which in methanol free electrolyte is at a minimum in the "double layer" capacity indicating that the shape of the methanol oxidation wave is mainly determined by the specific adsorption of Cl^-, the latter being present as an impurity in $HClO_4$ at a concentration of at least 10^{-7} M.

Based on chloride AES isotherms for Pt(111) and Pt(100) emersed from HF containing HCl, we have proposed a two-stage process for chloride adsorption on both surfaces. The maximum in the methanol oxidation current on both surfaces corresponds to the potential where the second stage of Cl^- adsorption is completed.

In H_2SO_4, the methanol oxidation peak on both Pt(111) and Pt(100) appears at a potential which in methanol-free electrolyte is significantly below the potential for the onset of "oxide" formation. The shape of methanol oxidation wave is

determined by the process of (bi) sulphate adsorption. A two-stage process for (bi) sulphate adsorption is also proposed. As with the electrolyte continuing the Cl^- ions, the maximum in the methanol oxidation current corresponds to the potential where the second stage of HSO_4^- ($SO_4^=$) adsorption is completed.

The inhibition of the rate of oxidation of methanol by chloride and (bi) sulphate ions is caused by a blocking of surface sites by ions adsorption, i.e. Chloride and sulphuric acid anion adsorption is predominant over the adsorption of methanol at the relative concentrations used in this work.

UPD Cu was found to have a very large inhibiting effect even at very low (< 10% monolayer) coverage. A possible explanation for this unusually large inhibiting effect at low coverage is the coupling of anion adsorption and Cu deposition resulting in induced anion adsorption onto Pt atoms neighboring the Cu adatoms. We suggest a mechanism for this induced anion adsorption in terms of local work function concept and the local pzc change of Pt atoms near the Cu ad-atoms.

ACKNOWLEDGMENT

This work was supported by the Assistant Secretary for Conservation and Renewable Energy, Office of Transportation Technologies, Electric and Hybrid Propulsion Division of the U.S. Department of Energy under Contract No. DE-AC03-76SF00098.

REFERENCES

1. K.R. Williams, M.R. Andrew and F. Jones, Hydrocarbon Fuel Cell Technology, ed. B.S. Baker (New York: Academic Press, 1965).

2. N.A. Hamton, M.J. Willars and B.D. McNicol, J. Power Sources, 1 (1981), 191.

3. B.D. McNicol, J. Electroanal. Chem., 118 (1981) 71.

4. M. Breiter and S. Gilman, J. Electrochemical Soc. 109 (1962) 622.

5. V.S. Bagotzky and Yu. B. Vassilyev, Electrochemica Acta, 12 (1967) 1323.

6. S. Gilman and M. Breiter, ibid, 109, (1962) 1099.

7. V.S. Bagotzky, Yu, B. Vassilyev and I.I. Pyshnograeva, Electrochemica Acta, 16 (1971) 2141.

8. R.R. Adzic, A.V. Tripkovic and W.O'Grady, Nature 296 (1982) 137.

9. J. Clavilier, C. Lamy and J.M. Leger, J. Electroanal. Chem. 125 (1981) 249.

10. A.V. Tripkovic and R.R. Adzic, Extended Abstracts, 38th. I.S.E. Meeting, Maastricht, Holland, 1981, No. 4.6.3.

11. S. Motoo and N. Furuya, J. Electroanal. Chem. 197 (1986) 209.

12. S.G. Sun and J. Clavilier, J. Electroanal. Chem., 236 (1987) 91.

13. B. Beden, S. Juanto, J.M. Leger and C. Lamy, J. Electroanal. Chem., 237 (1987) 119.

14. B. Beden, C. Lamy, A. Bewick and K. Kunimiju, J. Electroanal. Chem. 121 (1981) 343.

15. K. Kunimatsu, J. Electron. Spectroscopy 30 (1983) 215.

16. S. Wilhelm, T. Iwasita and W. Vielstich, J. Electroanal. Chem. 238 (1987) 385.

17. J. Willsau, O. Wolter and J. Heitbaum, J. Electroanal. Chem. 185 (1985) 163.

18. A. Norton-Haner and P.N. Ross, J. of Phys. Chem. 95 (1991) 3740 and reference therein.

19. M. Shibata and S. Motoo, J. Electroanal. Chem., 229 (1987) 381.

20. M. Beltowska-Brzezinska, J. Heitbaum and W. Vielstich, Electrochemica Acta 30 (1981) 1461.

21. E.P.M. Leiva and M.C. Giordano, J. Electrochem. Soc., 145 (1985) 87.

22. P.N. Ross and F.T. Wagner, in: Advances in Electrochemistry and Electrochemical Engineering, Vol. 13, Eds. H. Gerisher and C.W. Tobias (Wiley, New York, 1984) p.69.

23. N. Markovic, M. Hanson, G. McDougal and E. Yeager, J. Electroanal. Chem., 214 (1986) 555.

24. J. Clavilier, R. Durand and G. Guinet and R. Faure, J. Electroanal. Chem., 127 (1981) 281.

25. F.T. Wagner and P.N. Ross, J. Electroanal. Chem., 150 (1984) 141.

26. N. Markovic, N. Marinkovic and R. Adzic, J. Electroanal. Chem. 241 (1988) 309.

27. P. Fague, N. Markovic R. Adzic, C. Fieiro and E. Yeager, J. Electroanal. Chem. 289 (1990) 245.

28. P.N. Ross, Jr., Journal de Chimie Physique 88 (1991) 1353.

29. J. Clavilier, J. Electroanal Chem., 107 (1980) 211.

30. J. Clavilier, K. El. Achi and A. Rodes, Chemical Physics, 141 (1991).

31. N. Markovic and E. Yeager, unpublished results.

32. C. Lamy, J.M. Leger, J. Clavilier and R. Parsons, J. Electroanal Chem., 150 (1985) 71.

33. P.N. Ross, unpublished results.

34. R.C. Yeates, "The Characterization and Catalysis of Modified Platinum Surfaces", Ph.D. Thesis, Lawrence Berkeley Laboratory, 1985.

35. G. Garwood and A. Hubbard, Surf. Sci. 112 (1981) 281.

36. F. Wagner and P. Ross, J. Electroanal. Chem. 250 (1988) 301.

37. B. Cahan, H. Villullas and E. Yeager, J. Electroanal. Chem. 306 (1991) 213.

38. G. Horanyi, J. Solt and F. Nagy, J. Electroanal. Chem. 31 (1971) 95.

39. A. Wieckowski, P. Zelenay and K. Varga, J. Chimie Physique 88 (1991) 1247.

40. G. Horanyi, J. Electroanal. Chem. 55 (1974) 45; G. Horanyi and G. Vertes, J. Electroanal. Chem. 45 (1973) 291.

41. N. Markovic and P.N. Ross, Extended Abstracts, 181st Meeting of the Electrochemical Society in St. Louis, Missouri, May 17-22, 1992.

42. N. Markovic, M. Avramov-Ivic, N. Marinkovic and R. Adzic, J. Electroanal. Chem., 312 (1991) 115.

FIGURES

Fig. 1. Cyclic voltammograms for UHV-prepared and flame-annealed Pt(111) single crystals in 0.1 M $HClO_4$ (upper curves) and with 25 mM CH_3OH (lower curves).

Fig. 2. Cyclic voltammograms for flame annealed platinum single crystals in 0.1 M $HClO_4$ and 0.05 M H_2SO_4 with (lower curves) and without methanol (upper curves).

Fig. 3. Cyclic voltammogram for flame annealed Pt(111) in 0.1 M $HClO_4$ and 0.1 M KOH with (bottom) and without (top) 25 mM CH_3OH.

Fig. 4. Cyclic voltammograms for flame annealed Pt(111) in 0.1 M $HClO_4$ with additions of trace amounts of HCl [from ref. 31].

Fig. 5. Cyclic voltammograms for UHV-prepared Pt(111) in 0.3 M HF with addition of HCl (upper curves) and chloride/platinum AES peak ratio as a function of emersion potential (lower curves).

Fig. 6. The same as in Fig. 5 but for Pt(100).

Fig. 7. Cyclic voltammograms for flame annealed single crystals in 0.3 M HF with (solid curve) and without (dashed) curve 25 mM CH_3OH.

Fig. 8. Cyclic voltammograms for methanol oxidation on flame-annealed platinum single crystals in 0.1 M $HClO_4$ + 5×10^{-5} MCl.

Fig. 9. Cyclic voltammograms for methanol oxidation on flame-annealed platinum single crystals in 0.1 M $HClO_4$ with addition of HCl. Inserts: The effect of Cl^- ions on hydrogen adsorption/desorption pseudo-capacitance.

Fig. 10. Cyclic voltammograms for flame annealed single crystals as a function of H_2SO_4 concentration.

Fig. 11. Cyclic voltammograms for methanol oxidation on flame-annealed platinum single crystals in "clean" 0.1 M $HClO_4$, in 0.1 M $HClO_4$ with addition of HCl, and in 0.05 $MH_2\ SO_4$.

Fig. 12. Cyclic voltammograms for flame-annealed platinum single crystals in 0.1 M $HClO_4$; 0.1 M $HClO_4$ + 1×10^{-6} M Cu^{2+} (upper curves) and 0.1 M $HClO_4$ + 1×10^{-6} M Cu^{2+} + 25 mM CH_3OH (lower curves).

Fig. 13. The same as in Fig. 12 but for 0.05 MH_2SO_4.

Fig. 14. Cyclic voltammograms for flame-annealed Pt(111) single crystal in 0.05 M H_2SO_4 (upper curve) and potential dependance of corrected bisulfate simulate adsorption integrated band intensity IR spectra [from ref. 27].

Table 1. Absolute Coverages of Cu and Cl on Emersed Pt(111) Electrodes

AES Peaks	Peak Ratio	Calibration Factor	Atomic Ratio
Cl (181)/Cu (920)	15	4.5	3.3
Cu (920)/Pt (237)	0.2	3.7	0.05
Cl (181)/Pt (237)	2.5	16	0.15

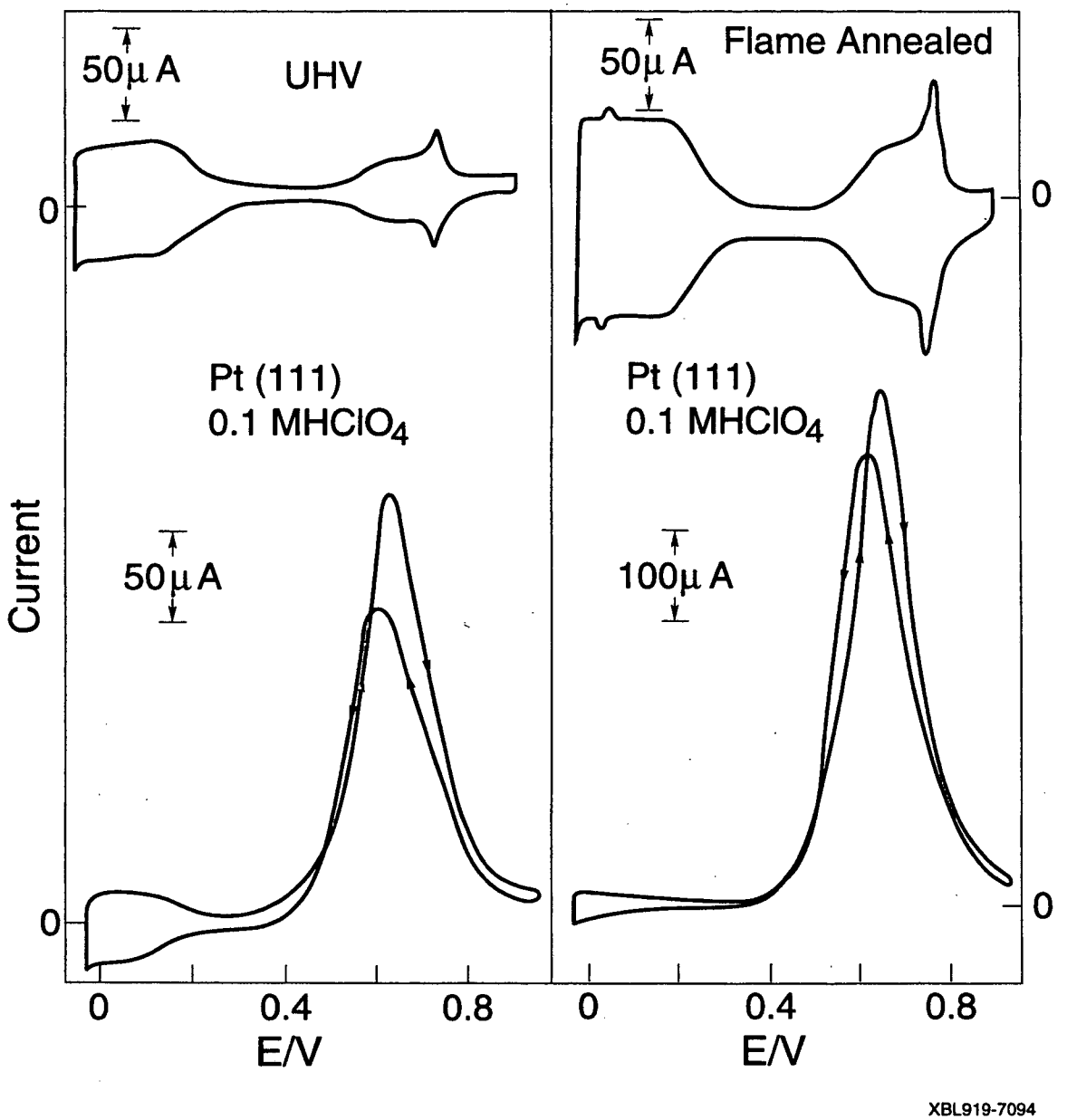
50μ A
UHV
0
Pt (111)
0.1 MHClO4
50μ A
Current
0
0
0.4
0.8
E/V
50μ A
Flame Annealed
0
Pt (111)
0.1 MHClO4
100μ A
0
0
0.4
0.8
E/V
XBL919-7094

Figure 1

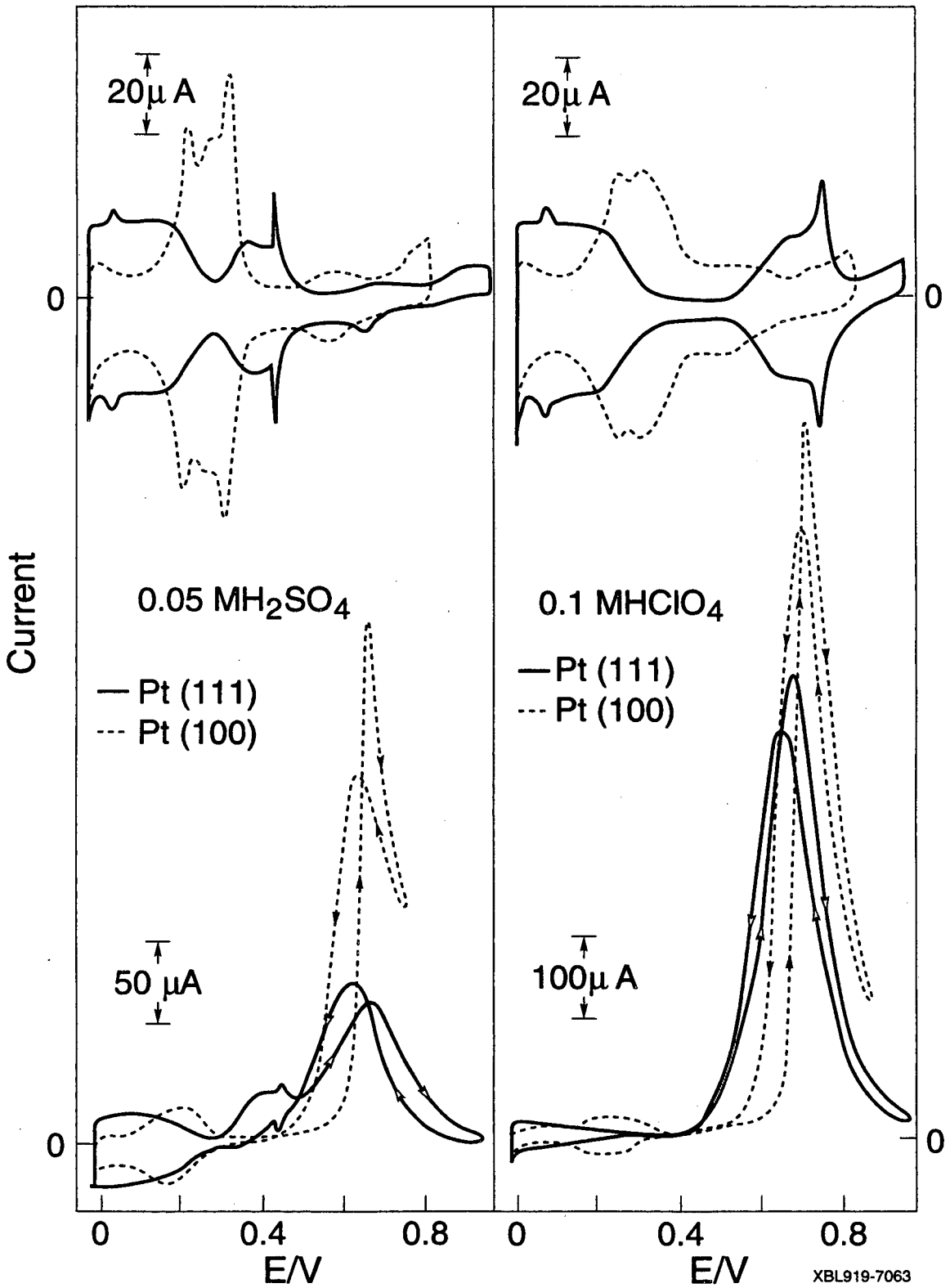
20μ A
20μ A
0
0
Current
0.05 MH2SO4
— Pt (111)
--- Pt (100)
0.1 MHClO4
—Pt (111)
--- Pt (100)
50 μA
100μ A
0
0
0
0.4
0.8
E/V
0
0.4
0.8
E/V
XBL919-7063

Figure 2

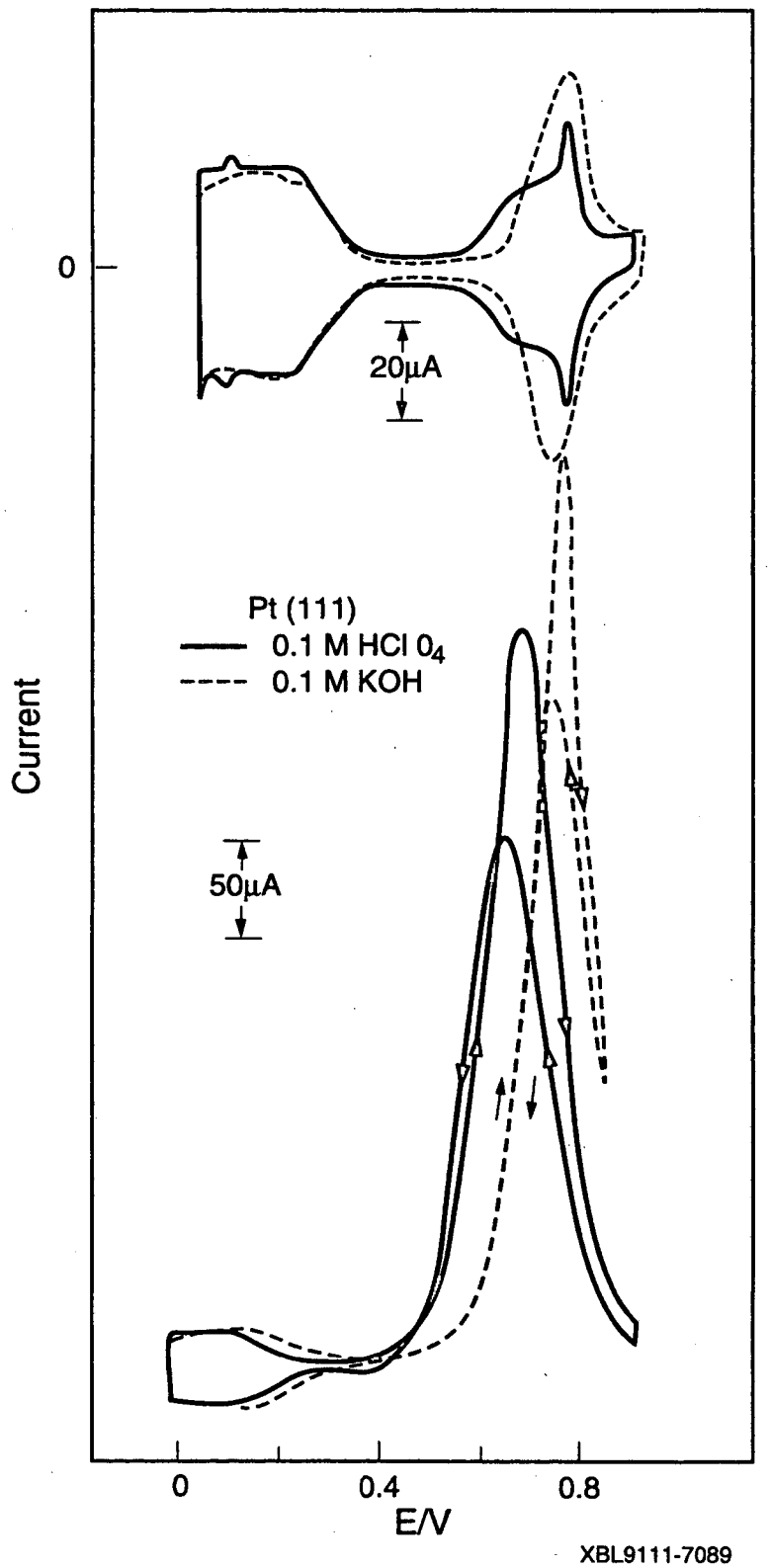
0
20μA
Pt (111)
0.1 M HCl 0_4
0.1 M KOH
Current
50μA
0
0.4
0.8
E/V
XBL9111-7089

Figure 3

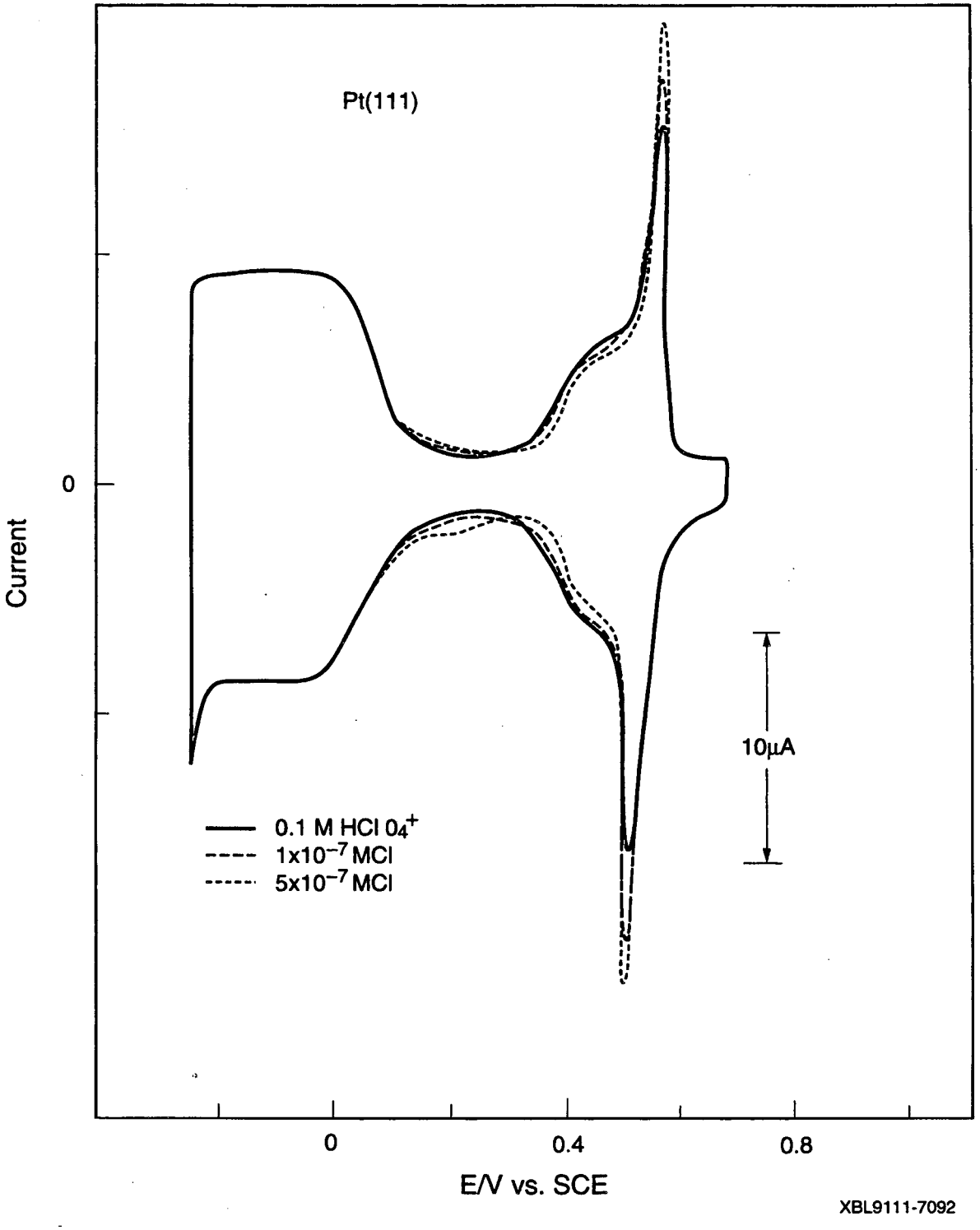
Pt(111)
Current
0
10μA
0.1 M HCl 0$_4^+$
1x10^{-7} MCl
5x10^{-7} MCl
0
0.4
0.8
E/V vs. SCE
XBL9111-7092

Figure 4

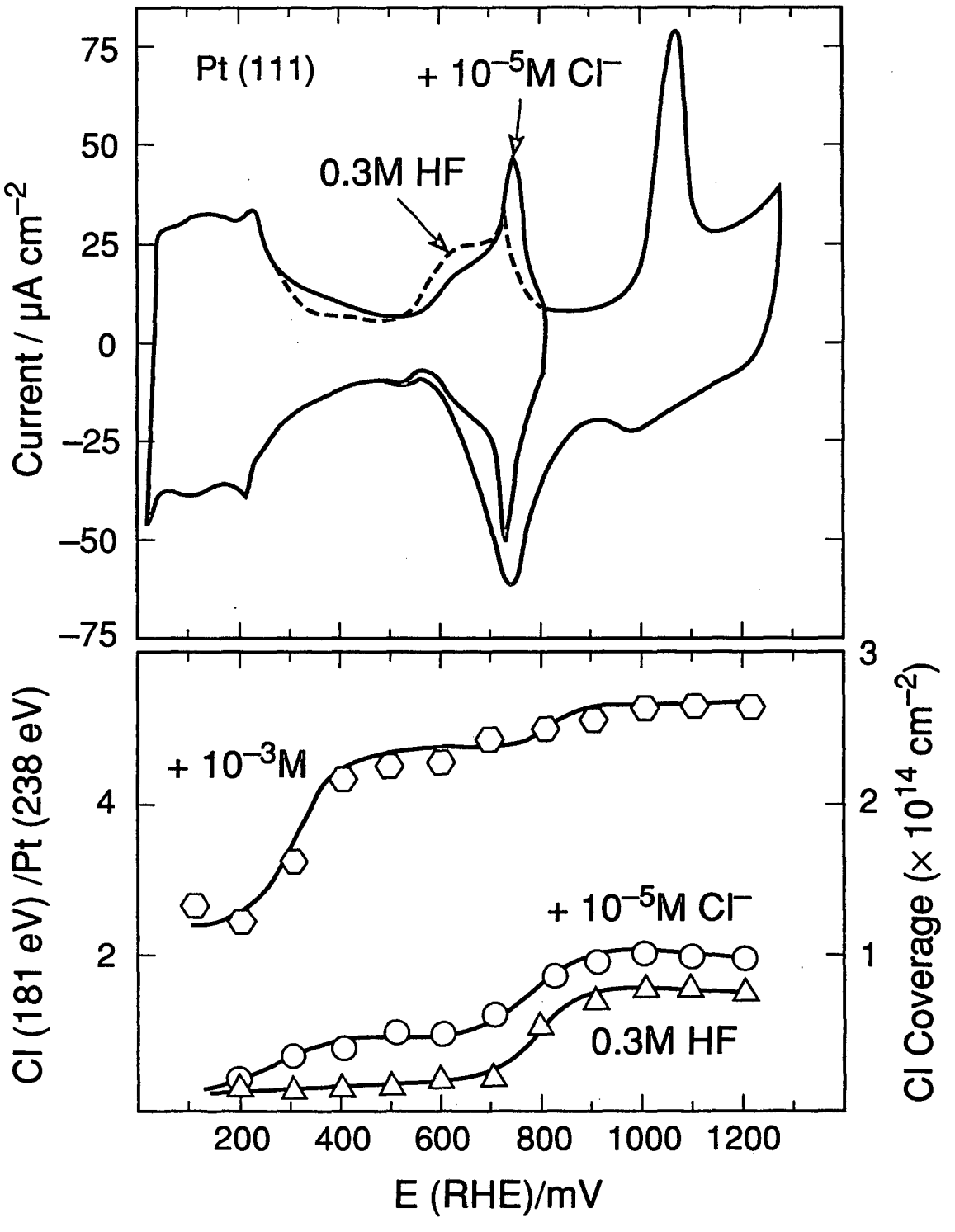

Figure 5

XBL 9110-6830

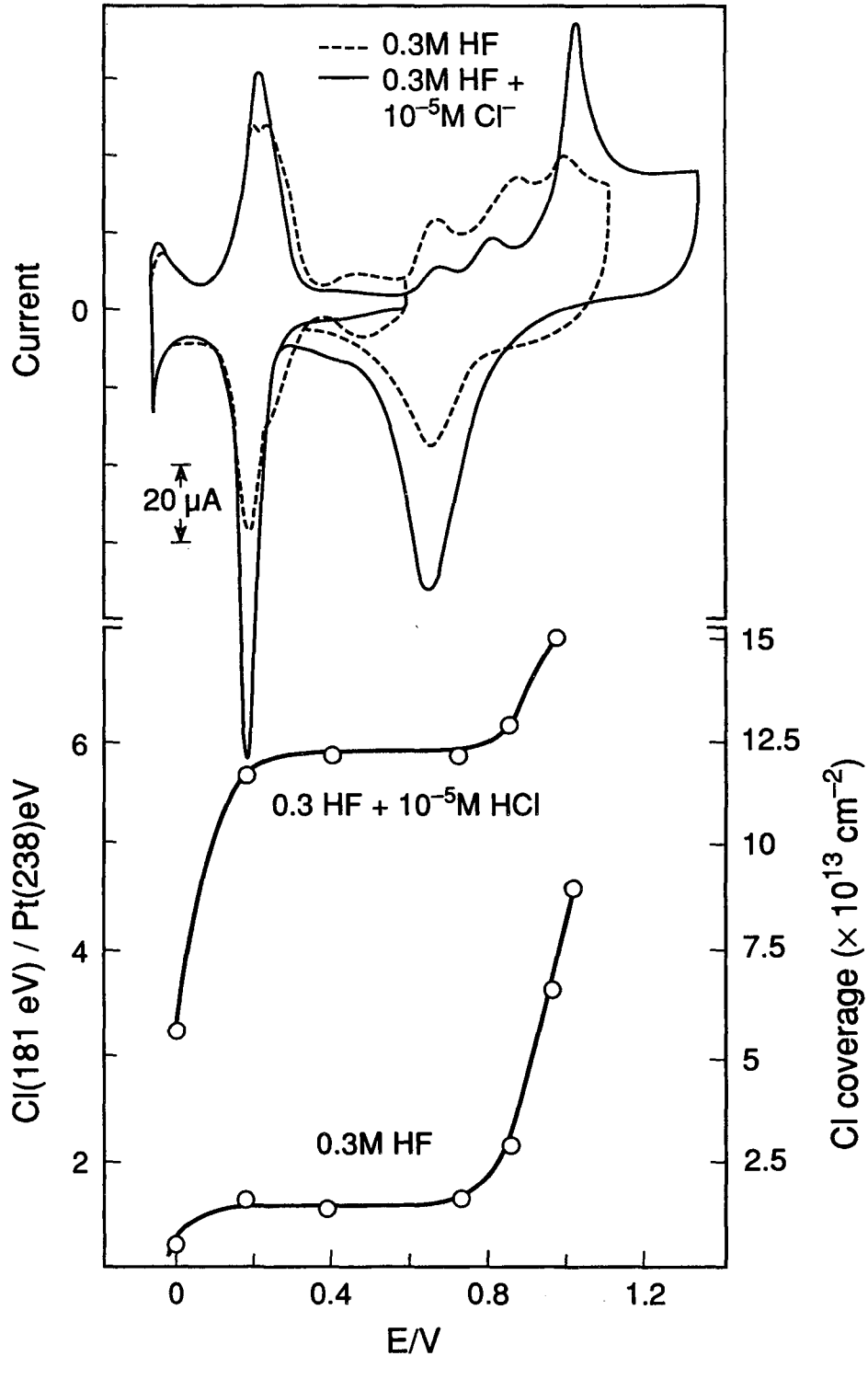

Figure 6 XBL 9110-6831

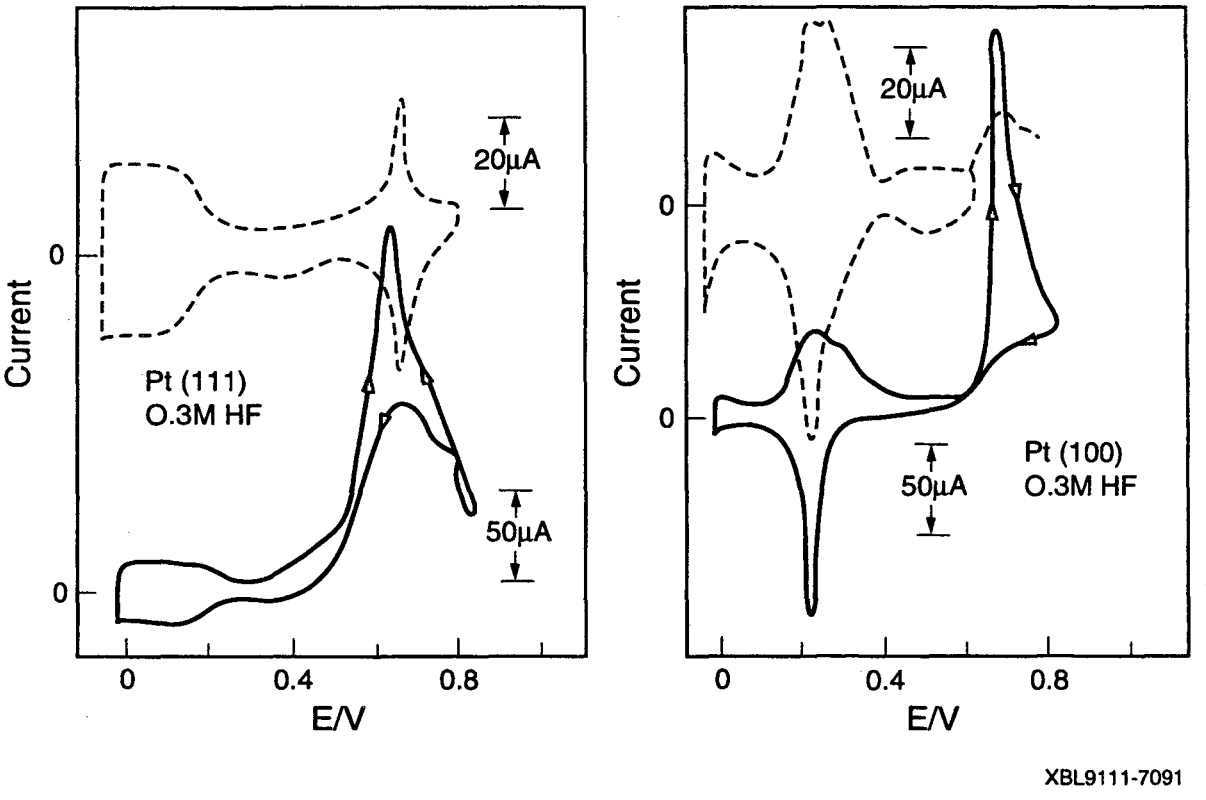
Current
0
0
20μA
Pt (111)
O.3M HF
50μA
0
0.4
0.8
E/V
Current
0
0
20μA
50μA
Pt (100)
O.3M HF
0
0.4
0.8
E/V
XBL9111-7091

Figure 7

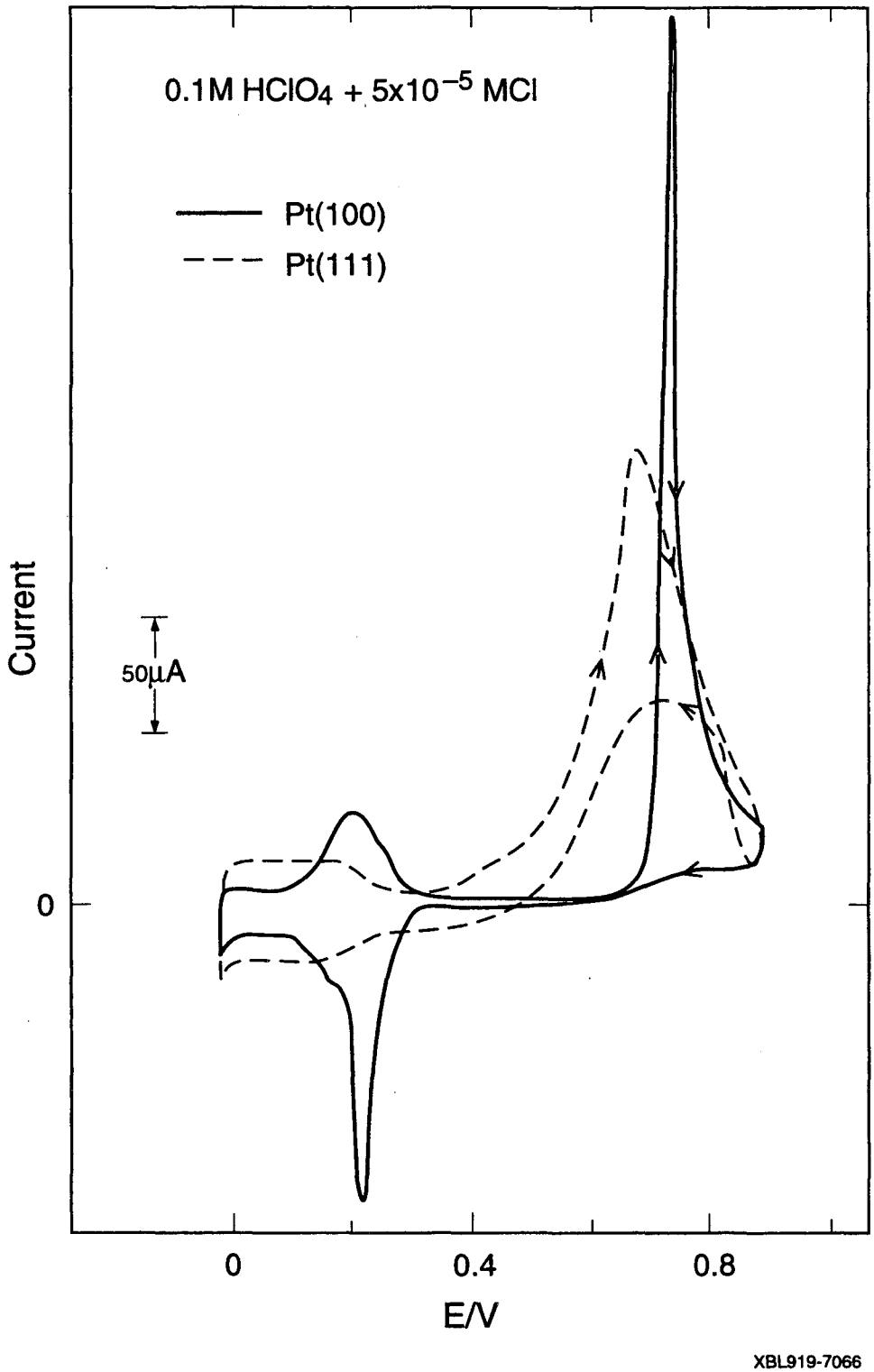
0.1M HClO4 + 5x10−5 MCl
Pt(100)
Pt(111)
Current
50μA
0
0
0.4
0.8
E/V
XBL919-7066

Figure 8

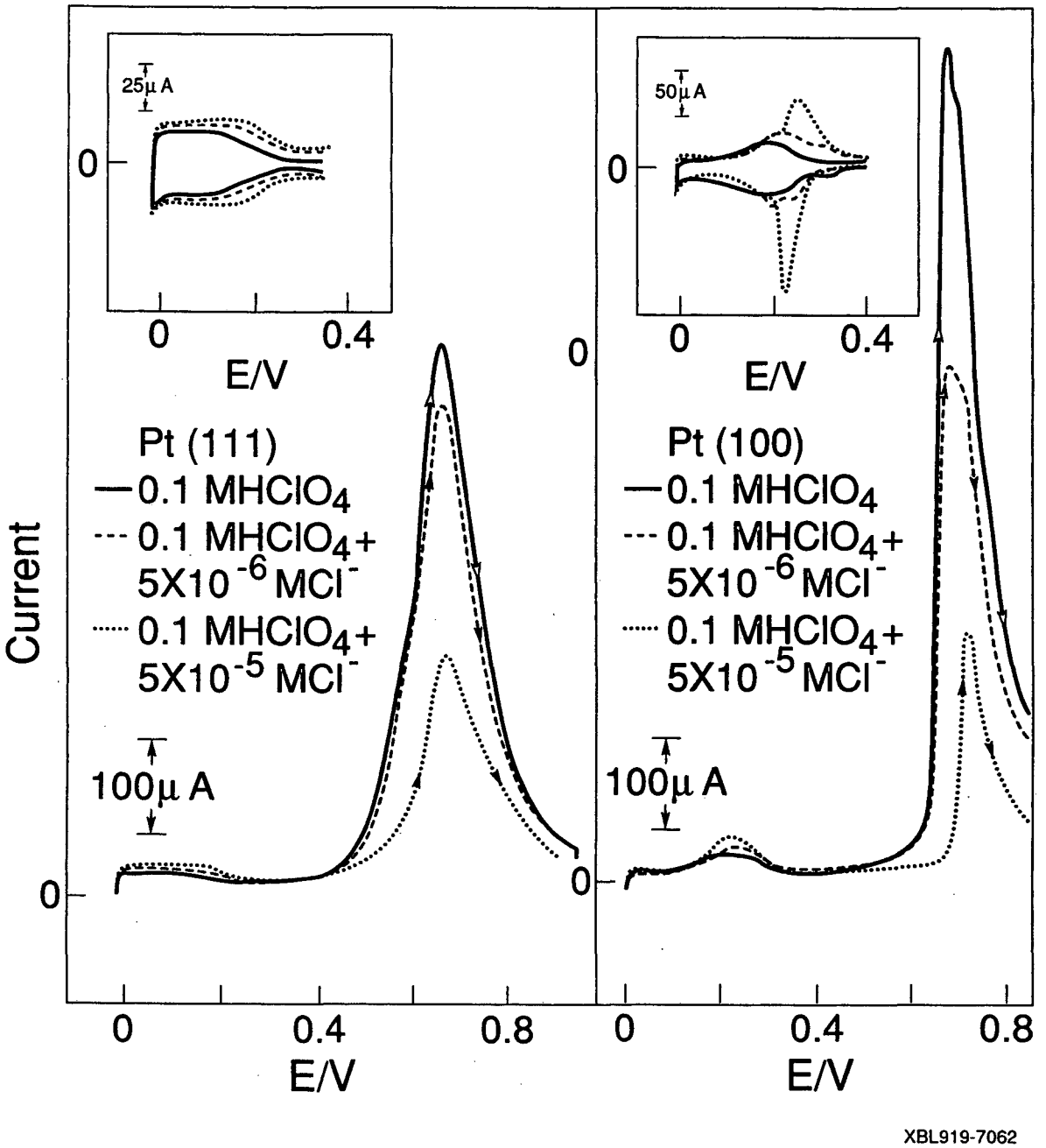
25μ A
0
0
0.4
E/V
Pt (111)
—0.1 MHClO4
--- 0.1 MHClO4+
5X10-6 MCl-
····· 0.1 MHClO4+
5X10-5 MCl-
100μ A
Current
0
0
0.4
0.8
E/V
50μ A
0
0
0.4
E/V
Pt (100)
—0.1 MHClO4
--- 0.1 MHClO4+
5X10-6 MCl-
····· 0.1 MHClO4+
5X10-5 MCl-
100μ A
0
0.4
0.8
E/V
XBL919-7062

Figure 9

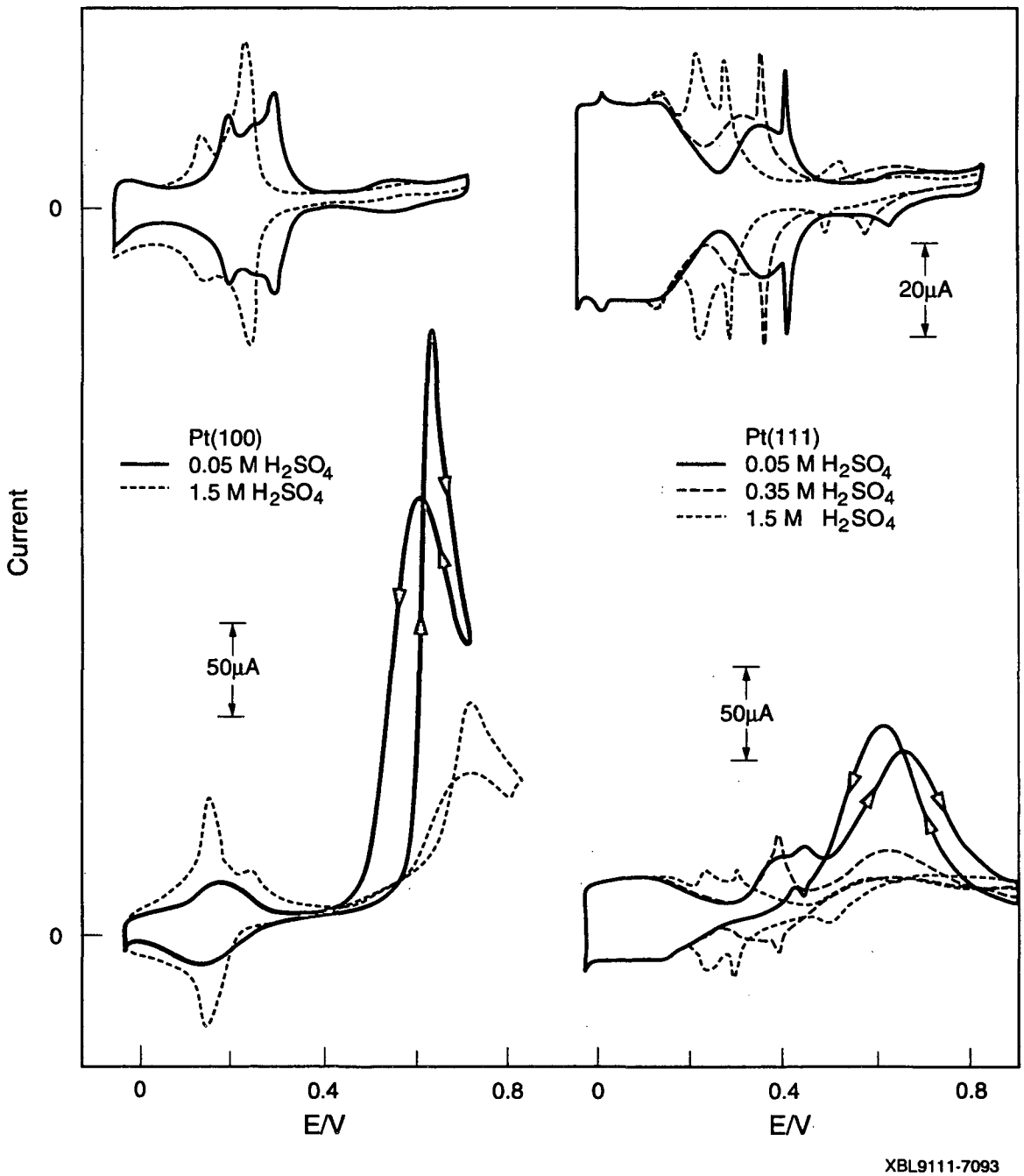
Current
0
0
Pt(100)
0.05 M H_2SO_4
1.5 M H_2SO_4
50μA
20μA
Pt(111)
0.05 M H_2SO_4
0.35 M H_2SO_4
1.5 M H_2SO_4
50μA
0
0.4
0.8
E/V
0
0.4
0.8
E/V
XBL9111-7093

Figure 10

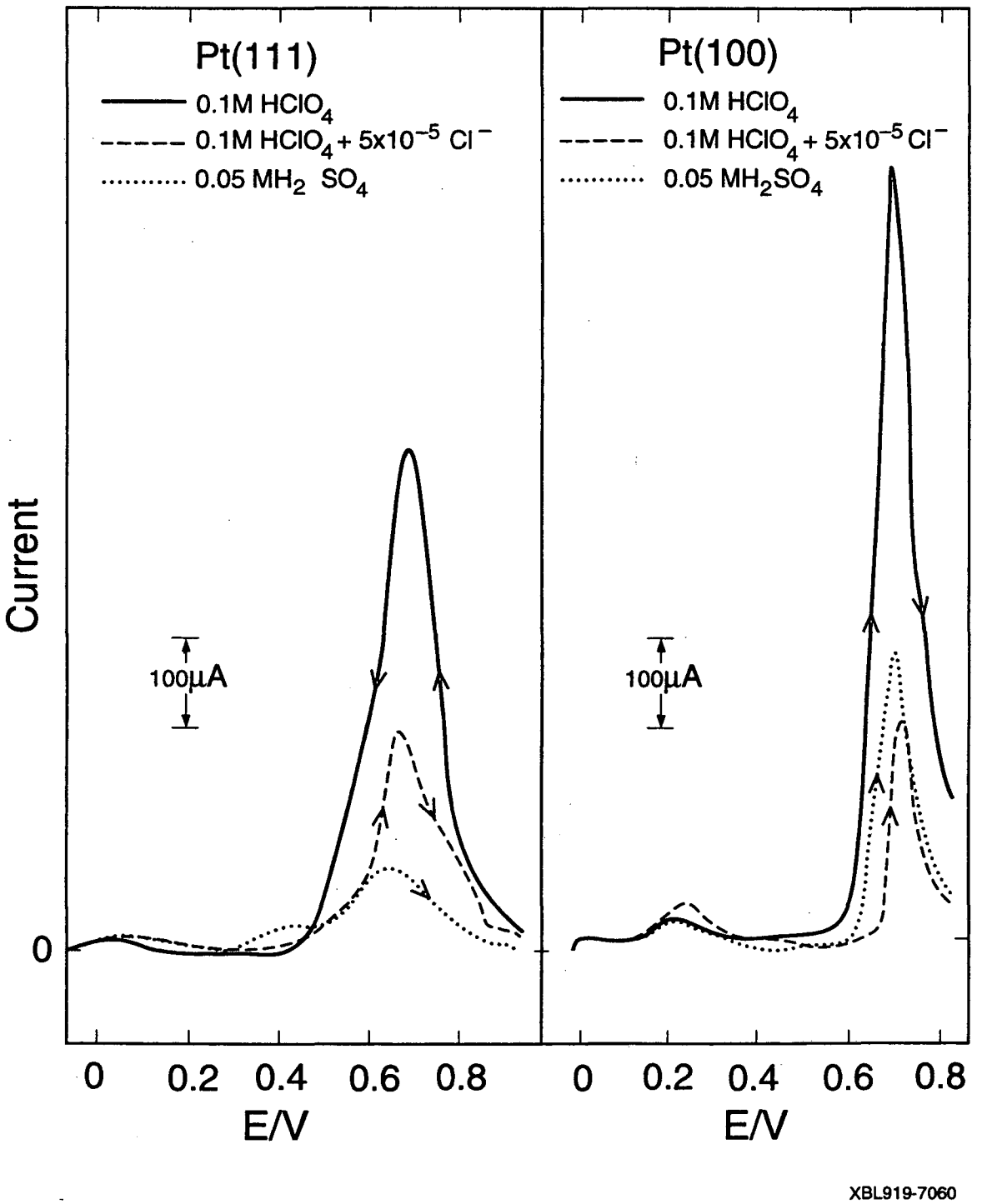
Pt(111)
0.1M $HClO_4$
0.1M $HClO_4$ + 5x10^{-5} Cl^-
0.05 MH_2 SO_4
Pt(100)
0.1M $HClO_4$
0.1M $HClO_4$ + 5x10^{-5} Cl^-
0.05 MH_2SO_4
Current
100μA
100μA
0
0 0.2 0.4 0.6 0.8
E/V
0 0.2 0.4 0.6 0.8
E/V
XBL919-7060

Figure 11

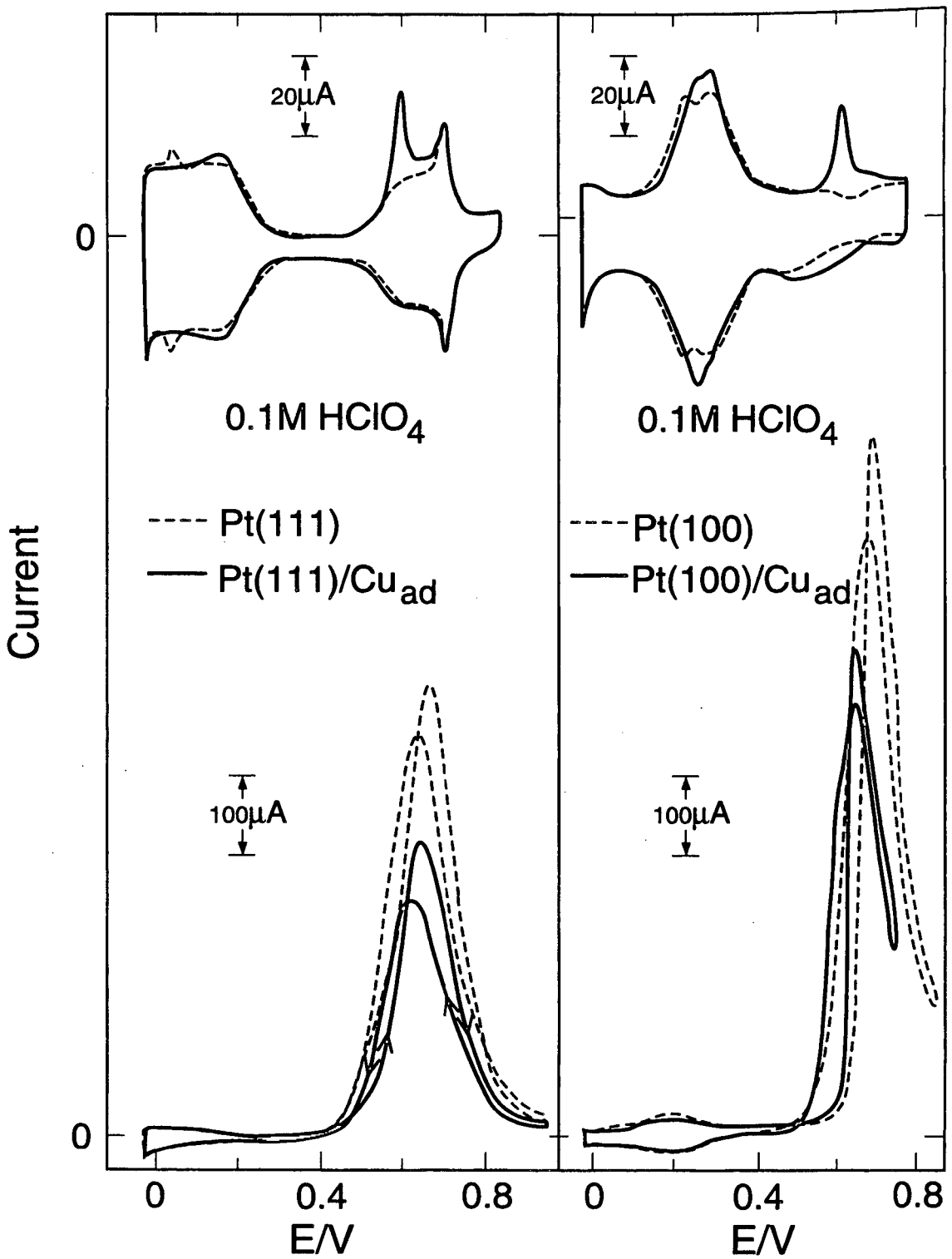

Figure 12

XBL919-7059

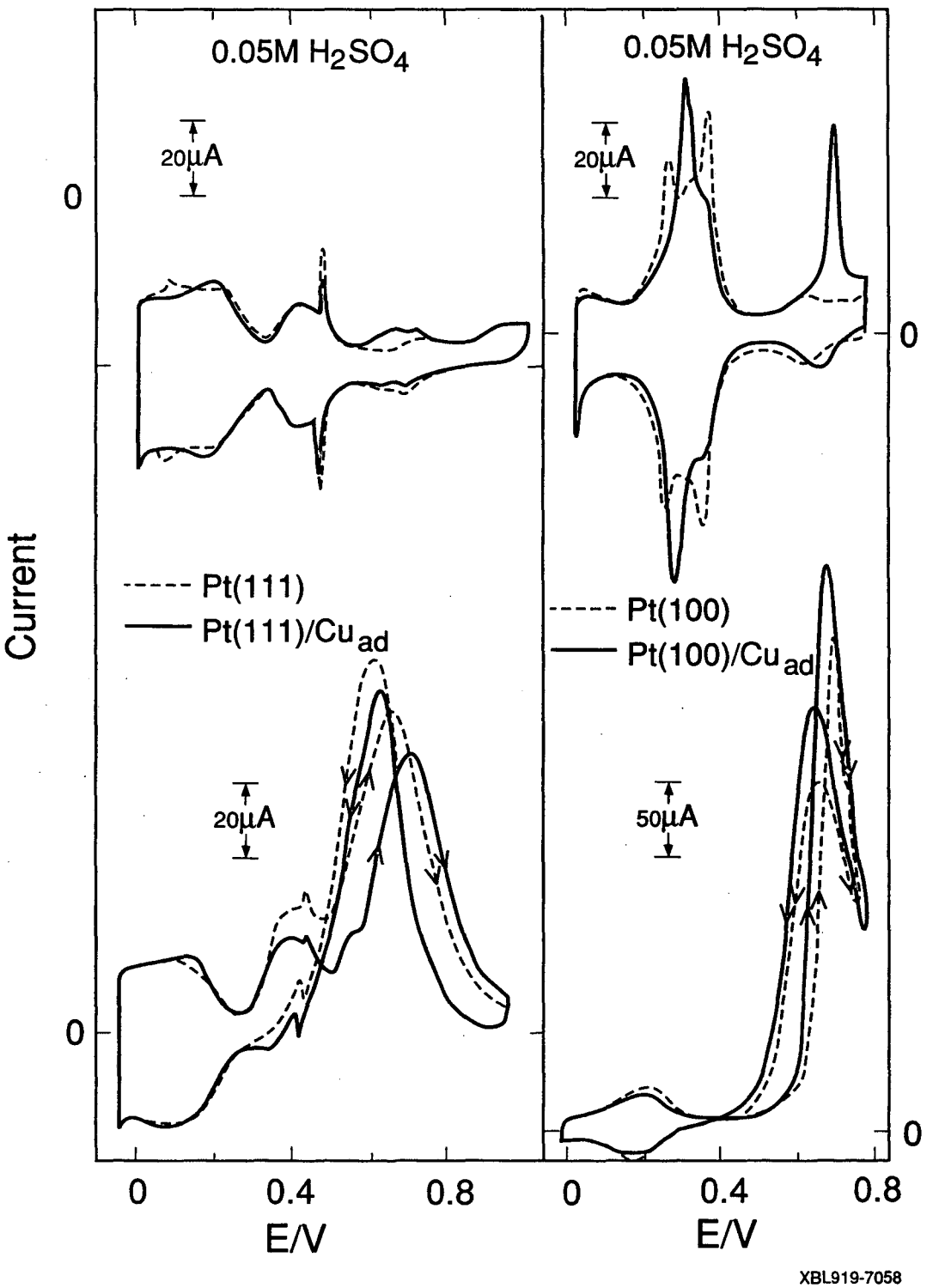
0.05M H_2SO_4
0.05M H_2SO_4
20μA
20μA
0
0
Current
----- Pt(111)
—— Pt(111)/Cu_{ad}
----- Pt(100)
—— Pt(100)/Cu_{ad}
20μA
50μA
0
0
0
0.4
0.8
E/V
0
0.4
0.8
E/V
XBL919-7058

Figure 13

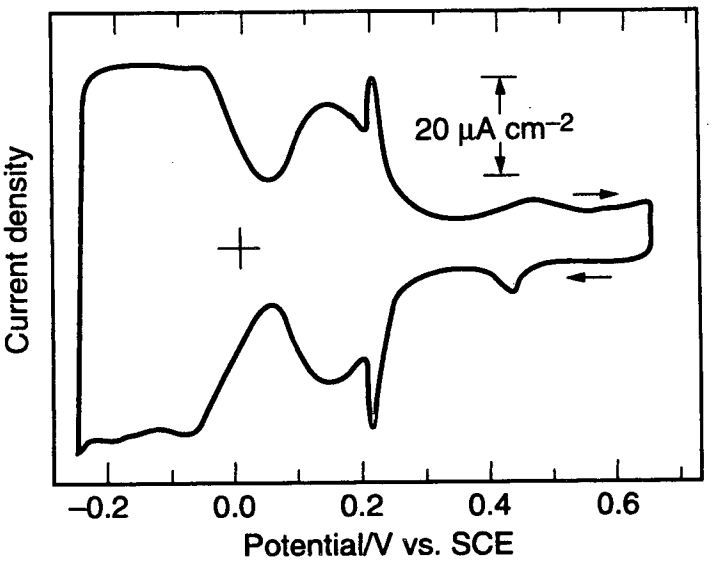
20 μA cm−2
Current density
−0.2
0.0
0.2
0.4
0.6
Potential/V vs. SCE

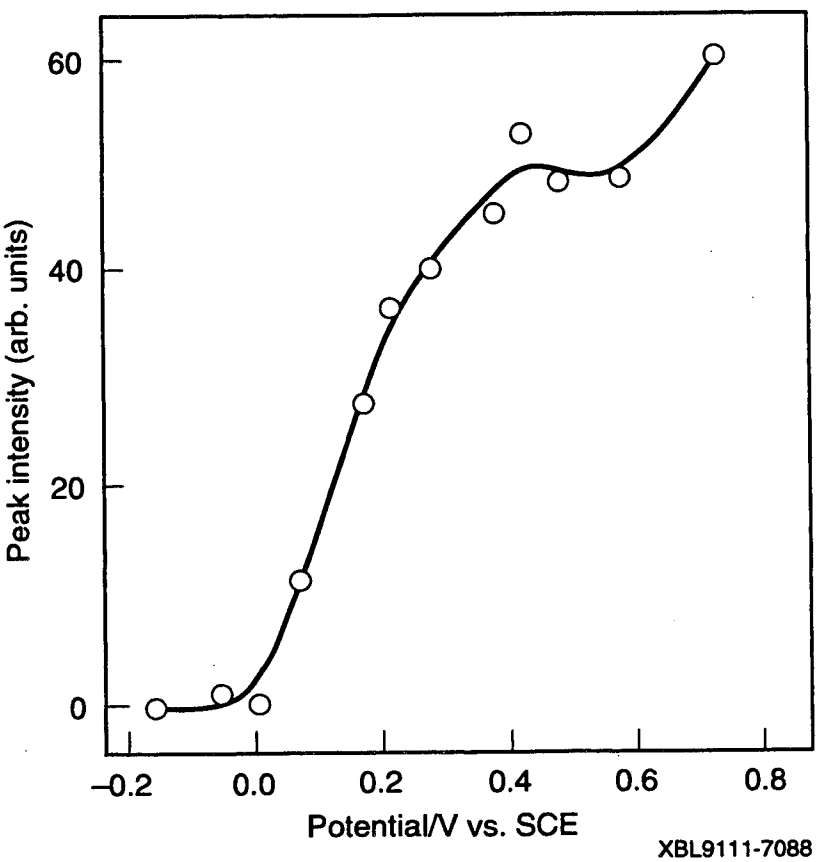
60
40
20
0
Peak intensity (arb. units)
−0.2
0.0
0.2
0.4
0.6
0.8
Potential/V vs. SCE
XBL9111-7088

Figure 14

LAWRENCE BERKELEY LABORATORY
UNIVERSITY OF CALIFORNIA
TECHNICAL INFORMATION DEPARTMENT
BERKELEY, CALIFORNIA 94720